EXACT CONSTRUCTIONS IN THE (NON-LINEAR) PLANAR THEORY OF ELASTICITY: FROM ELASTIC CRYSTALS TO NEMATIC ELASTOMERS

PIERLUIGI CESANA, FRANCESCO DELLA PORTA, ANGKANA RÜLAND, CHRISTIAN ZILLINGER, AND BARBARA ZWICKNAGL

ABSTRACT. In this article we deduce necessary and sufficient conditions for the presence of "Conti-type", highly symmetric, exactly-stress free constructions in the geometrically non-linear, planar n-well problem, generalising results of [CKZ17]. Passing to the limit $n \to \infty$, this allows us to treat solid crystals and nematic elastomer differential inclusions simultaneously. In particular, we recover and generalise (non-linear) planar tripole star type deformations which were experimentally observed in [MA80a, MA80b, KK91]. Further we discuss the corresponding geometrically linearised problem.

CONTENTS

1. Introduction 1
2. Main Results for the Finite N Case 6
3. Proofs for the Constructions for Finite N 18
4. The Limit $N \to \infty$ 31
5. Remarks on Three-Dimensional Constructions 41
Appendix A. Necessary Relation between the Radius of the Outer Polygon and the Radius of the Inner Polygon: the Solutions to (31) 46
Appendix B. Proof of Corollary 2.4 48
Appendix C. Reduction to Cauchy-Green Tensors used in the Proof of Proposition 2.6 49
Acknowledgements 50
References 50

1. INTRODUCTION

It is the purpose of this article to discuss certain specific, stress-free constructions for two-dimensional models of shape-memory alloys and nematic liquid crystal elastomers in a unified mathematical framework. Both of these physical systems can be described by highly non-quasi-convex energies within the calculus of variations, which formally share important features and give rise to complex and wild microstructures. Before turning to our mathematical results, let us thus first describe the physical background of these models, discussing their common features and the problems we are interested in.

1.1. Elastic crystals.

Shape-memory alloys are solid, elastic crystals which undergo a first order, diffusionless solid-solid phase transformation in which symmetry is reduced upon the passage from the high temperature phase, *austenite*, to the low temperature phase, *martensite*. Due to the loss of symmetry there are typically various, energetically equivalent *variants of martensite* in the low temperature phase. Mathematically, shape memory alloys have been very successfully modelled within

a variational framework introduced by Ball and James [BJ87], where it is assumed that the observed deformations of a material minimise an energy functional of the form

$$\int_\Omega W(\nabla u, \theta) dx. \tag{1}$$

Here $\Omega \subset \mathbb{R}^3$ denotes the reference configuration, which is typically chosen to be the material in the austenite phase at a fixed temperature, $u : \Omega \subset \mathbb{R}^3 \to \mathbb{R}^3$ is the deformation of the material, $\theta : \Omega \to (0, \infty)$ represents temperature and $W : \mathbb{R}^{3\times 3} \times \mathbb{R}_+ \to \mathbb{R}_+$ is the stored energy density. Physical requirements on the stored energy density are

- *frame indifference*, which implies that
$$W(QF) = W(F) \text{ for all } Q \in SO(3),$$
- *invariance under material symmetries*, by which
$$W(FX) = W(F) \text{ for all } X \in \mathcal{P}.$$
Here $\mathcal{P}$ denotes the point group of austenite, which is a (discrete) subgroup of $SO(3)$.

These two conditions render the described models for martensitic phase transformations highly *non-linear*, *non-quasi-convex* and give rise to rich microstructures [Bha03]. The above two conditions on W in particular determine the associated *energy wells* $K(\theta)$, which are characterised by the condition

$$W(F, \theta) = 0 \text{ iff } F \in K(\theta).$$

Typically, $K(\theta)$ is of the form

$$K(\theta) = \begin{cases} \alpha(\theta)SO(3) \text{ for } \theta > \theta_c, \\ \alpha(\theta)SO(3) \cup \bigcup_{j=1}^m SO(3)U_j(\theta) \text{ for } \theta = \theta_c, \\ \bigcup_{j=1}^m SO(3)U_j(\theta) \text{ for } \theta < \theta_c, \end{cases} \tag{2}$$

where $\theta_c \in (0, \infty)$ denotes the transformation temperature, $\alpha(\theta) : (0, \infty) \to \mathbb{R}_+$ is a thermal expansion coefficient, $\alpha(\theta)SO(3)$ models the austenite phase (taken as the reference configuration at the critical temperature, i.e. $\alpha(\theta_c) = 1$) and $SO(3)U_j(\theta)$ represents the respective variants of martensite, where $U_j(\theta) \in \mathbb{R}^{3\times 3}$, see [Bal04]. Here the matrices $U_j(\theta)$ are obtained through the action of the symmetry group from $U_1(\theta)$, i.e. for each $j \in \{1, \dots, m\}$ there exists $P \in \mathcal{P}$ such that

$$U_j(\theta) = PU_1(\theta)P^T.$$

Due to the complicated and highly non-linear and non-convex structure of the energies in (1), a commonly used first step towards the analysis of low energy microstructures in martensitic phase transformations is the analysis of the differential inclusion

$$\nabla u \in K(\theta), \tag{3}$$

which corresponds to the determination of *exactly stress-free* states. A class of particularly symmetric, exactly stress-free deformations had been studied by Conti [Con08] in specific set-ups (we will also refer to these as "Conti constructions"), see also the precursors in [MŠ99, CT05]. It is the purpose of this article to study these structures systematically in the sequel, following and extending ideas from [CKZ17] and treating elastic and nematic liquid crystal elastomers in a unified framework.

1.2. **From elastic crystals to nematic elastomers.** Nematic liquid crystal elastomers (NLCEs) are a class of *soft* shape-memory alloys where shape-recovery is accompanied by the emergence of soft modes and mechanical and optical instabilities. Constitutively, NLCEs are rubber-like elastic materials composed of cross-linked polymeric chains incorporating molecules of a nematic liquid crystal. We refer to [WT03] for an extensive description of the synthesis and physical properties of NLCEs. The complicated interaction between orientation of the liquid crystal molecules (described by $\hat{n}(x)$, a unit vector field called the director) and the macroscopic strain field generated by the polymeric chains may induce optical isotropy, low-order states of the nematic molecules and shear-banding of martensitic type. As a typical signature of the nematic-elastic coupling, NLCEs spontaneously deform when an assigned orientation is imposed (for instance, by an external electric field) to the liquid crystal molecules. Conversely, a macroscopic deformation induces a rotation and re-orientation of the nematic molecules in a way that the director tends to be parallel to the direction of the largest principal stretch associated with the deformation.

Let us comment on the passage from solid to nematic liquid crystal elastomers. Despite the profound differences in the nature of elastic crystals (martensite) and nematic-elastomers it turns out that the morphology of the microstructures observed in both these materials may be modelled with the language of continuum mechanics by means of multi-well energies of a similar – at least formally – structure and shape yielding in both cases highly non-quasi-convex variational problems.

In the context of NLCE typical stored energy densities may be considered in the general form [ADMD15]

(4)
$$W(F) := \sum_{j=1}^{N} \frac{d_j}{\gamma_j} \left[\left(\frac{\lambda_1(F)}{c_1} \right)^{\gamma_j} + \left(\frac{\lambda_2(F)}{c_2} \right)^{\gamma_j} + \left(\frac{\lambda_3(F)}{c_3} \right)^{\gamma_j} - 3 \right], \text{ if } \det(F) = 1,$$

and $+\infty$, if $\det F \neq 1$. The matrix $F \in \mathbb{R}^{3\times 3}$ denotes the deformation gradient of the material and $\lambda_k(F)$ are its ordered singular values, that is, the square root of the eigenvalues of the matrix FF^T, under the assumption $0 < \lambda_1 \leq \lambda_2 \leq \lambda_3$. Finally, $0 < c_1 \leq c_2 \leq c_3 < \infty$ as well as d_j and $\gamma_j \in [2, \infty)$ are constants.

Stored energy densities of the form (4) comprise the classical energy model for NLCEs of Bladon, Warner and Terentjev (BWT) [BWT94] which is obtained by setting $N = 1, \gamma_j = 2, d_j = \mu$ (shear modulus) and $c_1 = c_2 = r^{-1/6}, c_3 = r^{1/3}$ (where $r > 1$ is the backbone anisotropy parameter) into (4). By operating this substitution we obtain the BWT energy density which we write – with some abuse of notation – as

$$W(F) = \frac{\mu}{2} \left[r^{1/3} \lambda_1^2(F) + r^{1/3} \lambda_2^2(F) + \frac{\lambda_3^2(F)}{r^{2/3}} - 3 \right]. \tag{5}$$

Moreover, $W(F) = \min_{\hat{n}\in\mathbb{S}^2} \tilde{W}(F, \hat{n})$, where

(6)
$$\tilde{W}(F, \hat{n}) = \frac{\mu}{2} \left(r^{1/3} \left[\operatorname{tr}(FF^T) - \frac{r-1}{r} FF^T \hat{n} \cdot \hat{n} \right] - 3 \right) \quad \text{if } \det(F) = 1, \hat{n} \in \mathbb{S}^2$$

(and extended to $+\infty$ if $\det(F) \neq 1$ or $\hat{n} \notin \mathbb{S}^2$) and $\hat{n}$ is the nematic director. Notice in (6) the energy density is constant if we replace $\hat{n}$ with $-\hat{n}$: this is the so-called head-tail symmetry of nematic liquid crystals, a fundamental physical property which is incorporated in all the most typical models of both nematic liquid and solid-liquid crystals including the ones discussed here.

Similarly as in the elastic crystal setting in shape-memory materials, in studying minimisers of (4) or (5) a first commonly used approach is to consider the associated differential inclusion describing exactly stress-free states. In the case of (4) this leads to the study of the following problem:

$$\nabla u \in K_\infty := \{F \in \mathbb{R}^{3\times 3};\ \det(F) = 1, \lambda_k(F) = c_k, k \in \{1,2,3\}\}, \tag{7}$$

where K_∞ corresponds to the zero-energy level of W. Observe that $W \geq 0$ and $W(F) = 0$ if and only if $F \in K_\infty$. In contrast to the finite number of wells in the elastic crystal case, one is now confronted with an infinite number of energy wells.

This is evident if we investigate the zero-energy level of $\tilde{W}(F, \hat{n})$. Simple algebraic computations show that $\min_{F,\hat{n}} \tilde{W}(F, \hat{n}) = 0$ and that the minimum is achieved by any pair $(\overline{F}, \overline{n})$ such that $\lambda_1 = \lambda_2 = r^{-1/6}, \lambda_3 = r^{1/3}$ and $\overline{n}$ coincides with the eigenvector associated with the largest eigenvalue of $\overline{F}\overline{F}^T$ or, equivalently, by any pair $(U_{\hat{n}}, \hat{n})$ where $\hat{n}$ is any vector in $\mathbb{S}^2$ and

$$U_{\hat{n}} = r^{1/3}\hat{n} \otimes \hat{n} + r^{-1/6}(Id - \hat{n} \otimes \hat{n}), \tag{8}$$

where $Id \in \mathbb{R}^{3\times 3}$ is the identity matrix. Deformations of the form stated in equation (8), which are the equivalent of the bain strain in martensite, correspond to a spontaneous distortion of a ball of radius one into a prolate ellipsoid whose major axis (of length $r^{1/3}$) is parallel to $\hat{n}$. For the NLCE model of (5) the energy well is obtained by plugging $c_1 = c_2 = r^{-1/6}, c_3 = r^{1/3}$ into K_∞ (see (7)) which leads to the differential inclusion

$$\nabla u \in \tilde{K}_\infty(r) = \bigcup_{\hat{n}\in\mathbb{S}^2} SO(3)U_{\hat{n}}. \tag{9}$$

Equation (9) is resemblant of the situation described by the equations (2)-(3) for martensite, where one has replaced $\mathcal{P}$, the (discrete) point group of the material with the full group $SO(3)$. This is indeed the striking property of NLCE models: The stored energy is invariant under rotations in the ambient space as well as under the action of $SO(3)$.

This formal similarity of the two problems suggests that they can be analysed in similar frameworks. In Lemma 4.5 we show that the set (7) can be obtained as the limit $n \to \infty$ of sets of the type (2). Moreover, even for finite $n \in \mathbb{N}$ the sets from (2) are always subsets of the set K_∞, hence any solution obtained for finite n is also always a solution to the differential inclusion problem for (7) in a corresponding n-gon domain. This could for instance be exploited in numerical benchmarking (see the discussion at the end of Section 4.1). Due to these similarities, in the sequel we seek to discuss the two physical systems simultaneously.

A series of experiments and technological implementations which appeared over the last three decades have inspired and motivated an extensive body of work on the modelling and design of microstructure formation in NLCEs. Examples which are particularly relevant in our context at the interface between solid crystals and nematic liquid crystal elastomers are the formation of martensitic-type stripe-domains (experimentally observed in [KF95], analysed under the assumptions of large non-linear deformations in [DD02] and infinitesimal displacements in [Ces10]), respectively, and complex configurations where optical microstructure interacts in a collaborative fashion with instabilities induced by geometrical constraints, such as wrinkling (modeled in [CPB15], images of the prototypes designed at NASA Langley Research Center are reported in [PB16]).

Although planar and radial configurations such as the one in Figure 9 to the best of our knowledge have not been observed in NLCEs, we hope the theoretical results and constructions described in this article will inspire further experimental investigation of complex microstructure morphology in NLCEs.

1.3. **Main results.** The objective of this article is the unified study of a specific class of planar solutions to differential inclusions of the forms (3), (7) and (9) at a fixed temperature $\theta > 0$ and for planar geometries. These type of deformations had been introduced by Conti [Con08], see also [Pom10] and the constructions in [Kir03]. Deformations and materials allowing for this class of constructions are of particular interest due to various reasons. Indeed, from a physical point of view

- materials which allow for these deformations are candidates for low hysteresis materials;
- the constructions are motivated by specific deformation fields observed experimentally (e.g. tripole star deformations).

Moreover, in addition to these physical sources of interest, also from a purely mathematical point of view these constructions are relevant, as

- they can be used as building block constructions in convex integration schemes,
- the deformations occur both in the theory of elastic crystals and also in models for nematic liquid crystal elastomers. This allows for a unified mathematical discussion of both systems.

Let us comment on some of these aspects in more detail:

On the one hand, these specific solutions are of particular interest as not only their bulk energy vanishes, but also their surface energy, measured for instance in terms of the BV norm of ∇u is finite (see Section 2.4 for some remarks on energetics). As a consequence, materials which exhibit such structures are candidates for materials with *low hysteresis* as nucleation has low energy barriers (both in purely bulk but also in bulk and surface energy models) [CKZ17], see also [ZRM09] for more information on hysteresis in shape-memory alloys.

On the other hand, in addition to their relevance in the analysis of hysteresis, microstructures of this type are often used as key building blocks in the construction of convex integration solutions. As the energies in (1), (4) and (5) are typically highly non-quasi-convex and thus in particular not immediately amenable to the direct method in the calculus of variations, it came as a surprise, when it was discovered (first in the context of shape-memory alloys, later – see [ADMD15] – also in the context of nematic liquid crystal elastomers) that for a large set of possible boundary conditions exact solutions to (3), (7) and (9) exist (see [MŠ99, Kir03] and the references therein). These solutions are obtained through iterative procedures in which oscillatory building blocks successively improve the construction, pushing it to become a solution to (3) in the limit. For more information on this we refer to [DM12, Dac07, MŠ98, CDK07, Kir03, KMŠ03, ADMD15, Rül16] and the references therein. The solutions which we discuss below are frequently used as building blocks [Con08, Kir03] in this context; they can even be applied in the *quantitative* analysis of convex integration solutions [RZZ19, RZZ18, RTZ18].

Motivated by these considerations, in this note we seek to:

- Extend the necessary and sufficient conditions for the presence of planar Conti-type constructions derived in [CKZ17] to arbitrary $n \in \mathbb{N}$. In particular, we reproduce the experimentally observed tripole star structures (both in the geometrically linearised and the non-linear theories). As a consequence, we also underline the observation from [KK91] that within a geometrically non-linear theory tripole stars in shape-memory alloys are not exactly stress-free. Yet, in a model involving elastic and surface energy contributions, we show that in certain regimes the tripole star deformations are of very low energy and thus candidates for energy minimizers (see Section 2.4). An interesting aspect from the modeling point of view, these

microstructures are planar and therefore fully covered by the 2D analysis we develop. However, in contrast to the experimentalists' point of view who interpret these microstructures as *disclinations*, we offer an interpretation of these configurations as *stressed microstructures* with low (elastic and surface) energy (see the discussion in Section 2.4).
- Pass to the limit $n \to \infty$. Physically this limit corresponds to the passage from solid crystals to nematic elastomers. Our results can hence also be read as predictions on microstructure formation for experiments on nematic elastomers in highly symmetric domains (where the symmetry of the domains may possibly serve as a *selection mechanism* for choosing a *finite number* of the possible set of infinitely many wells). This might also be of interest in numerical benchmarking (see the discussion at the end of Section 4.1).

To this end, we rely on the geometrically non-linear constructions from [CKZ17] which we investigate for a general n-well problem before passing to the limit $n \to \infty$. As in [CKZ17] we obtain necessary and sufficient conditions on the wells in order for the corresponding Conti constructions to exist. We remark that in the context of the two-dimensional, geometrically linearised hexagonal-to-rhombic phase transformation by completely different methods (relying on the characterisation of homogeneous deformations involving four variants of martensite) necessary conditions had been derived in an OxPDE summer project by Stuart Patching [Pat14]. The sufficiency of the necessary conditions had previously been established in [CPL14] in the geometrically linearised hexagonal-to-rhombic phase transformation. The results in [CPL14] are also complemented by numerical simulations of possible solutions, which match the experimentally observed solutions in [MA80a, MA80b, KK91] well.

1.4. **Organisation of the article.** The remainder of the article is organised as follows: We begin by presenting our main results and their physical implication on the construction for the geometrically non-linear n-well problem in Section 2. This includes a discussion of necessary and sufficient conditions for a single layer construction (Section 2.1.1-2.1.3), an iteration of single layer constructions to more complex concatenated structures (Section 2.2) with small stresses, its geometrically linearised counterpart (Section 2.3) and finally a discussion of the physically observed "tripole star" structures (Section 2.4). The proofs of these results are presented in Section 3. In Section 4 we then show that the nematic liquid elastomer inclusion problem can also be embedded into this framework by passing to the limit $n \to \infty$ both in the geometrically non-linear (Section 4.1) and the geometrically linearised situations (Section 4.3). In this context we relate the special boundary conditions which had been chosen in [ADMD15] (see Section 4.3) to our differential inclusions. Finally, in Section 5 we comment on our (negative) results on analogous three-dimensional constructions and conclude the article by an appendix, in which we provide a number of auxiliary results.

2. Main Results for the Finite N Case

In this section we discuss necessary and sufficient conditions for (iterated) Conti-type constructions which may serve as physically relevant, highly symmetric nucleation mechanisms (Section 2.1). To this end, we first discuss the set-up of the problem and systematically derive necessary and sufficient conditions for the sought for solutions for a single layer construction (Section 2.1.3). Subsequently, we iterate these structures and show that here necessarily small stresses occur in the geometrically non-linear theory (which matches experimental observations of disclinations in similar structures), see Section 2.2.

After the discussion of the non-linear construction, we recall and analyse its geometrically *linearised* counterpart in Section 2.3. Here *no* stresses are present in the iterated structures which become even more symmetric than in the geometrically non-linear theory. Hence, while capturing the geometry of these low energy deformations, the linearised theory does *not* reflect the energetics of the nonlinear setting very precisely (in that no stresses are present).

In Section 2.4 we discuss the physical significance of the described Conti-type deformations by considering the example of the experimentally observed tripole star structures.

2.1. **The single layer non-linear construction in a regular n-gon.** In this section, we both informally and formally introduce a class of possible "Conti-type" nucleation mechanisms (Sections 2.1.1 and 2.1.2) and provide necessary and sufficient conditions for these (Section 2.1.3).

2.1.1. *Set-up and problem formulation for a single layer construction – informal discussion.* We begin by discussing a single layer, low energy, highly symmetric nucleation construction. Let us first describe this informally. We are interested in studying a class of essentially two-dimensional deformations which we assume to originate from three-dimensional phase transformation by projection. Special physical settings which we have in mind are the experimental results from [KK91] where in the third component of the three-dimensional deformation gradients are affine. After this reduction to two dimensions, we consider deformations with the following properties (see Figures 1 and 3):

- Outside of a large regular n-gon Ω_n^E and inside of a small regular n-gon Ω_n^I, both with the same barycenter, the deformation is equal to a rotation (without loss of generality, we may assume it to be equal to the identity in the outside domain and a non-trivial rotation in the inner n-gon). Without loss of generality, we further assume that the barycenter of both n-gons is the origin.
- In the set $\Omega_n^E \setminus \Omega_n^I$ the deformation is piecewise constant on a set of triangles formed by connecting the vertices of Ω_n^E and Ω_n^I (see Figures 1 and 3).
- We require that the deformation is associated with a phase transformation, i.e. that the piecewise constant deformation gradients in $\Omega_n^E \setminus \Omega_n^I$ only attain values in the set $\bigcup_{j=1}^{m} SO(2)U_j$, where $U_j = PU_1P^T$ for some $P \in \mathcal{P}_n$ and $U_1 \in \mathbb{R}^{2\times 2}_{sym}$ and where $\mathcal{P}_n \subset O(2)$ denotes the point group of the transformation at hand. The presence of the group $O(2)$ instead of the more commonly observed group $SO(2)$ in the definition of the point group is a consequence of the projection from the three- to the two-dimensional set-up.
- We require that the deformation is volume preserving.

Having fixed the outer n-gon Ω_n^E, the condition on the volume preservation together with the fact that the deformation gradient has a constant determinant in $\Omega_n^E \setminus \Omega_n^I$ implies that after fixing a single vertex with coordinates (x_1, x_2) of the inner n-gon, the deformation u is already determined. Indeed, in order to ensure the volume preservation constraint, under the deformation u the vertex has to be mapped to the deformed vertex $R_*(x_1, x_2)$, where R_* is a rotation by $\frac{2\pi}{n}(1-2\alpha)$ and $\alpha \in (0, 1)$ denotes the angle of rotation of the inner n-gon with respect to the outer one (see Figures 2 and 3). Hence, in principle, the deformation u is determined by two parameters (e.g. the coordinates $(x_1, x_2) \in \mathbb{R}^2$). As in [CKZ17], we thus consider the two-parameter family of deformations given by

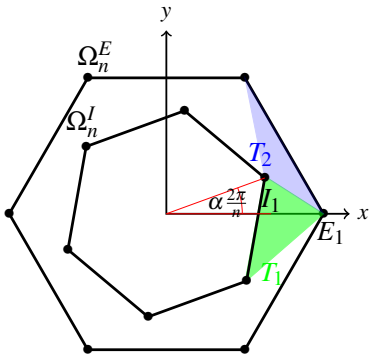

FIGURE 1. The inner and outer polygons are rotated by an angle $\frac{2\pi}{n}\alpha$ with respect to each other.

$$(\bar{a},\psi)\mapsto Id+\bar{a}\begin{pmatrix}\sin(\psi)\\ \cos(\psi)\end{pmatrix}\otimes\begin{pmatrix}-\cos(\psi)\\ \sin(\psi)\end{pmatrix}, \tag{10}$$

where $Id\in\mathbb{R}^{2\times 2}$ denotes the identity matrix and $\psi\in(0,2\pi]$. This is motivated by investigating the described deformations with austenite boundary conditions corresponding to low hysteresis deformations (in fact to allow for simpler computations, in the sequel, we will often replace the identity boundary conditions by boundary conditions given by a fixed rotation). As in [CKZ17] we will prove that the requirement that the deformation is associated with a phase transformation reduces the degrees of freedom from *two* parameters to a *single* parameter.

2.1.2. *Set-up and precise problem formulation for a single layer construction.* After the previous informal discussion of our problem, we present the formal problem set-up. We start by introducing the following definition: Here and below, for any set $A\subset\mathbb{R}^2$ we denote by A^{co} its convex hull and by $\operatorname{int}A$ its interior. Furthermore, by $\{e_1,e_2\}$ we denote an orthonormal basis of $\mathbb{R}^2$. We define the inner and outer vertices of our $n-$gons:

Definition 2.1. *Let $n\in\mathbb{N}, n\geq 2$, $\alpha\in(0,1]$ and $r_I,r_E\in(0,+\infty)$ with $r_I<r_E$. We say that $\Omega_n\subset\mathbb{R}^2$ is an $n-$*gon configuration *if, given*

$$E_i=r_E\cos\Big(\frac{2\pi}{n}(i-1)\Big)e_1+r_E\sin\Big(\frac{2\pi}{n}(i-1)\Big)e_2,\qquad i=1,\dots,n,$$
$$I_i=r_I\cos\Big(\frac{2\pi}{n}(i-1)+\alpha\frac{2\pi}{n}\Big)e_1+r_I\sin\Big(\frac{2\pi}{n}(i-1)+\alpha\frac{2\pi}{n}\Big)e_2,\qquad i=1,\dots,n,$$

and

$$\Omega_n^E=\{E_1,\dots,E_n\}^{co},\qquad \Omega_n^I=\{I_1,\dots,I_n\}^{co},$$

we have $\Omega_n:=\operatorname{int}\big(\Omega_n^E\setminus\Omega_n^I\big)$.

Given three points $p_1,p_2,p_3\in\mathbb{R}^2$, we denote by $\widehat{p_1p_2p_3}$ the open triangle $\widehat{p_1p_2p_3}=\operatorname{int}\{p_1,p_2,p_3\}^{co}$, and by $\overline{p_1p_2}$ the vector $\overline{p_1p_2}=p_2-p_1$. Finally, we denote by e_{ij} the unit vector $e_{ij}=\frac{\overline{E_jI_i}}{|\overline{E_jI_i}|}$. Now, given an $n-$gon configuration Ω_n as in Definition 2.1, we define the internal triangles T_i as

$$T_i=\begin{cases}E_{\frac{i+1}{2}}\widehat{I_{\frac{i-1}{2}}I_{\frac{i+1}{2}}}, & \text{if } i \text{ odd},\\ E_{\frac{i}{2}}\widehat{I_{\frac{i}{2}}E_{1+\frac{i}{2}}}, & \text{if } i \text{ even},\end{cases}$$

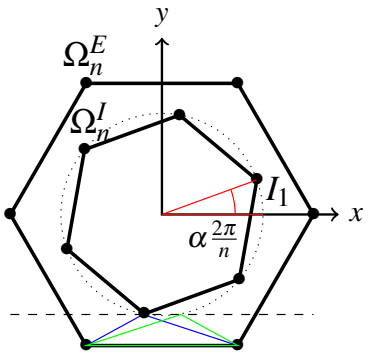

FIGURE 2. The "flipping" condition which is formalised in (iv). In order to ensure volume preservation an outer blue triangle in the reference configuration (see the online version for the colours) is mapped to the green outer triangle in the deformed domain. Assuming the deformation to be a rotation in the inner n-gon Ω_n^I, this is the only possible deformation that preserves the volume of the outer triangles. We also refer to Figure 3 for another illustration of the "flipping" condition.

where we use the convention that $E_{n+1} = E_1$ and $I_0 = I_n$.

With this notation in hand, we now consider the following problem:

Problem: Find $u \in W^{1,\infty}_{loc}(\mathbb{R}^2;\mathbb{R}^2)$ such that

(i) for every $i = 1, \dots, 2n$, u is affine on T_i;
(ii) $u = \mathrm{Id}$ on $\mathbb{R}^2 \setminus \Omega_n^E$, where Id denotes the identity map;
(iii) $\nabla u(x) \in \bigcup_{P\in\mathcal{P}_n} SO(2)PUP^T$ for some $U \in \mathbb{R}^{2\times 2}$ and for almost every $x \in \Omega_n^E \setminus \Omega_n^I$, where $\mathcal{P}_n \subset O(2)$ denotes the discrete (to be determined) symmetry group of our problem; in particular $\det(\nabla u(x)) = 1$;
(iv) $u(x) = R_* x$ in Ω_n^I, for some $R_* \in SO(2)$ of angle $\rho_n = \frac{2\pi}{n}\big(1 - 2\alpha\big)$. As a consequence, $R_* I_n = \Big(\cos\Big(\alpha\frac{2\pi}{n}\Big)e_1 - \sin\Big(\alpha\frac{2\pi}{n}\Big)e_2\Big)$.

We remark that these conditions formalise the requirements of a "Conti construction" with symmetry. These are piecewise affine deformations (as stated in (i)) with specific linear boundary conditions (ii) such that all involved deformation gradients are symmetry related as in (iii). The condition (iv) is a consequence of the desired symmetry of the n-gon configuration in conjunction with the prescription of the identity boundary data in (ii). Indeed, by requiring austenite boundary data, we infer that $\det(\nabla u) = 1$ on each triangle T_i, which can only be the case if R_* is of the described form. It corresponds to a "flipping" of the coordinates of I_n, see Figures 2 and 3.

In order to fix ideas, we introduce the symmetry group $\mathcal{P}_n$ which will naturally appear in the discussion of our problem in the sequel. It will turn out that the symmetry group $\mathcal{P}_n = \mathcal{R}_1^n \cup \mathcal{R}_2^n$ associated with our problem is a conjugated version of the dihedral group, i.e. of the symmetry group of a regular n-gon. More precisely, the standard dihedral group of a regular n-gon is given by

$$\hat{\mathcal{P}}_n := \hat{\mathcal{R}}_1^n \cup \hat{\mathcal{R}}_2^n. \tag{11}$$

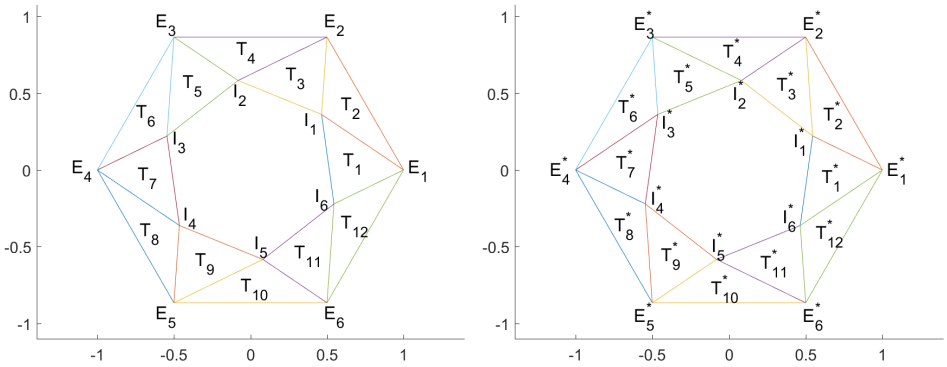

(A) (B)

FIGURE 3. Example of $n-$gon with $n = 6$. On the left before the action of the map u, on the right after its action. Here, we denoted by E_i^*, I_i^*, T_i^* the quantities $u(E_i), u(I_i), u(T_i)$. In order to ensure volume preservation, a necessary condition is the "flipping" of the triangles on which ∇u is constant which is formalised in condition (iv) in our problem formulation.

Here $\hat{\mathcal{R}}_1^n$ is the collection of all rotations leaving the n-gon invariant, i.e.

$$\hat{\mathcal{R}}_1^n := \left\{ \begin{pmatrix} \cos(\varphi_j) & \sin(\varphi_j) \\ -\sin(\varphi_j) & \cos(\varphi_j) \end{pmatrix} : \varphi_j = \frac{2\pi j}{n},\ j \in \{0, \dots, n-1\} \right\},$$

and $\hat{\mathcal{R}}_2^n$ is the collection of the corresponding reflections $\hat{\mathcal{R}}_2^n := \begin{pmatrix} 1 & 0 \\ 0 & -1 \end{pmatrix} \mathcal{R}_1^n$. In our problem, we will encounter a conjugated version of this, where

$$\begin{aligned} \mathcal{R}_2^n &:= \begin{pmatrix} e_{11} & e_{11}^\perp \end{pmatrix} \hat{\mathcal{R}}_2^n \begin{pmatrix} e_{11} & e_{11}^\perp \end{pmatrix} = \begin{pmatrix} e_{11} & e_{11}^\perp \end{pmatrix} \begin{pmatrix} 1 & 0 \\ 0 & -1 \end{pmatrix} \hat{\mathcal{R}}_1^n \begin{pmatrix} e_{11} & e_{11}^\perp \end{pmatrix}^T \\ &= (e_{11} \otimes e_{11} - e_{11}^\perp \otimes e_{11}^\perp) \hat{\mathcal{R}}_1^n \end{aligned}$$

and e_{11} denotes the vector defined in Section 2.1.2. We further note that $\hat{\mathcal{R}}_1^n$ is invariant under the change of basis to $(e_{11}\ e_{11}^\perp)$ since $SO(2)$ is commutative. Hence, the symmetry group in our problem

$$\mathcal{P}_n := \begin{pmatrix} e_{11} & e_{11}^\perp \end{pmatrix} \left(\hat{\mathcal{R}}_1^n \cup \begin{pmatrix} 1 & 0 \\ 0 & -1 \end{pmatrix} \hat{\mathcal{R}}_1^n \right) \begin{pmatrix} e_{11} & e_{11}^\perp \end{pmatrix}^T =: \mathcal{R}_1^n \cup \mathcal{R}_2^n, \tag{12}$$

is given by the dihedral group (that is the symmetry group of the standard regular n-gon) conjugated with a change of basis $(e_{11}\ e_{11}^\perp)$.

2.1.3. *Necessary and sufficient conditions for a single layer construction.* As informally already explained, direct dimension counting arguments yield that the set of all deformations satisfying the conditions (i), (ii) and (iv) form a *two*-parameter family. However, condition (iii), which corresponds to the requirement of being associated with a physical phase transformation provides an additional constraint. In fact, in discussing the necessary and sufficient conditions for the existence of solutions to this problem, we show that as in [CKZ17] this condition reduces the *two*-parameter family of solutions to a *one*-parameter family of deformations:

Theorem 1. *Recall the notation introduced in Section 2.1.2.*

(i) *A necessary condition for the satisfaction of (i)–(iv) from the problem formulation in Section 2.1.2 in Ω_n is the condition that*

$$\phi := \arccos\big(e_{11}\cdot e_{n1}\big) = \frac{\phi_n}{2}, \tag{13}$$

where $\phi_n = \frac{n-2}{n}\pi$ is the interior angle at each corner of the regular n-gon. In particular, this entails the necessary condition that the transformation is represented by

$$\begin{aligned} U =& \frac{1}{\sqrt{(1+a^2)^2+(\tan\phi)^{-2}(1-a^2)^2}}\Big(a(1+a^2)e_{11}\otimes e_{11}+\\ &+\frac{1}{a}(1+a^2+(\tan\phi)^{-2}-2a^2(\tan\phi)^{-2}+a^4(\tan\phi)^{-2})e_{11}^{\perp}\otimes e_{11}^{\perp}+\\ &+a(\tan\phi)^{-1}(1-a^2)(e_{11}\otimes e_{11}^{\perp}+e_{11}^{\perp}\otimes e_{11})\Big) \end{aligned} \tag{14}$$

for some $a>0$, and where $e_{11}^{\perp}\in\mathbb{S}^1$ is such that $e_{11}^{\perp}\cdot e_{11}=0$, $e_{11}\times e_{11}^{\perp}>0$. The associated point group $\mathcal{P}_n$ is necessarily given by the group in (12). Finally,

$$\frac{r_I}{r_E} = \frac{1}{\cos\left(\frac{\pi}{n}\right)}\left(\cos\Big(\frac{\pi}{n}(1-2\alpha)\Big)-\sqrt{\sin\Big(\frac{\pi}{n}2\alpha\Big)\sin\Big(\frac{2\pi}{n}(1-\alpha)\Big)}\right), \tag{15}$$

and

$$a=\sqrt{\frac{\sin\left(\frac{2\pi}{n}(1-\alpha)\right)}{\sin\left(\frac{2\pi}{n}\alpha\right)}}, \tag{16}$$

where α is as in Definition 2.1.

(ii) *Conversely, let $a>0$, $\alpha\in(0,1)$, $r_E, r_I>0$ satisfy (15)–(16). Let also $U:=U(a)$ be as in (17). Then there exists a deformation u such that the problem from Section 2.1.2 has a solution with $\mathcal{P}_n$ given by (12), i.e. a deformation u which satisfies the conditions (i)–(iv) which had been formulated in Section 2.1.2.*

In particular, not every map of the form (10) gives rise to a deformation which can be associated with a phase transformation. Instead of a *two*-parameter family only a *one*-parameter family of deformations exists with these properties.

Remark 2.2. *We notice that for each fixed $n\geq 1$ (16) gives a one-to-one relation between $a>0$ and $\alpha\in(0,1)$. Indeed, $a(\alpha)$ is strictly monotone and $\lim_{\alpha\to 0}a(\alpha)=+\infty$ and $a(1)=0$. Moreover, we note that as expected from the conditions (i)-(iv), we have $a(\frac{1}{2})=1$.*

Remark 2.3. *We note that we chose a symmetric matrix U to represent the energy well as is common in the mechanics literature. For the ease of notation, we will later on justify (see Remark 3.2) that we can equivalently work with a different representative $H=RU$ with*

$$\begin{aligned} R =& \frac{1}{\sqrt{(1+a^2)^2+(\tan\phi)^{-2}(1-a^2)^2}}\Big((1+a^2)e_{11}\otimes e_{11}+(1+a^2)e_{11}^{\perp}\otimes e_{11}^{\perp}\Big)+\\ &+(\tan\phi)^{-1}(1-a^2)(e_{11}\otimes e_{11}^{\perp}-e_{11}^{\perp}\otimes e_{11})\in SO(2), \end{aligned}$$

which yields

$$H=H(a)=\Big(ae_{11}\otimes e_{11}+\frac{1}{a}e_{11}^{\perp}\otimes e_{11}^{\perp}+\frac{a^{-1}-a}{\tan\phi}e_{11}\otimes e_{11}^{\perp}\Big). \tag{17}$$

In order to further analyse the single layer construction and to eventually use it in a concatenated construction of multiple rings (see Figure 4), we prove that the map $u : \Omega_n \to \mathbb{R}^2$ constructed in Theorem 1 is highly symmetric.

Corollary 2.4. *Let $a > 0$, $\alpha \in (0,1)$, $r_E, r_I > 0$ satisfy (15)–(16). Then the map u constructed in Theorem 1 (ii) satisfies*

$$\begin{aligned} \nabla u|_{T_i} &= \nabla u|^T_{Q_{\frac{n-1}{2}} T_{i+1}}, \qquad \text{if } n \text{ odd}, \\ \nabla u|_{T_i} &= \nabla u|_{Q_{\frac{n}{2}} T_i}, \qquad \text{if } n \text{ even}, \end{aligned} \tag{18}$$

for any $i = 1, \dots, n$, and where Q_j is the rotation of angle $\frac{2\pi j}{n}$. In particular, the second formula in (18) implies that if n is even ∇u attains at most n different deformation gradients in $\Omega_n^E \setminus \overline{\Omega_n^I}$, while in the odd case it in general attains $2n$ different deformation gradients in $\Omega_n^E \setminus \overline{\Omega_n^I}$. Furthermore,

$$R_* Q_\alpha \nabla u|_{T_{i+1}} Q_\alpha^T = Q_1 \nabla u|_{T_i} Q_1^T, \qquad \text{for any odd } i = 1, \dots, n\ . \tag{19}$$

Remark 2.5. *We remark that the symmetry conditions inferred in Corollary 2.4 have important implications on both the single layer construction from this section and the concatenated iterated onion ring structures which will be discussed in the next subsection:*

- *(i) We first consider the identities in (18). These describe a symmetry of the constructed deformation gradients in* each individual *"onion ring". Depending on whether n is even or odd, the deformation gradients in triangles which are "opposite" to each other (i.e. on T_i and $Q_{\frac{n-1}{2}} T_{i+1}$ if n is odd, or in T_i and $Q_{\frac{n}{2}} T_i$ if n is even) are related by either transposition or are directly equal (see Figure 4 for the labelling of the triangles).*

  This shows that if n is odd, a single onion ring involves up to $2n$ different deformation gradients, while if n is even, it only involves at most n deformation gradients. The fact that in the odd case "opposite" deformation gradients are related by transposition will play a significant role in the geometrically linearised transformation. Indeed, it will entail that in the linearised setting at most n different strain values are necessary for analogous constructions (both if n is even or if n is odd).
- *(ii) Next, the condition in (19) can be interpreted as comparing two adjacent deformations in* two different but consecutive *layers (as for instance in the triangles T_1 and T_{24} in Figure 4, see the following section for the formula of the concatenated construction). The right hand side corresponds to a deformation in a triangle T_i of the outer onion ring, while the left hand side corresponds to the deformation in the inner onion ring (see the definition (21) for v_n). The expression in (19) thus states that these two adjacent deformation gradients have the same value (see Figure 4). A numerical illustration of this is given in Figures 5 for tripole star structures and in Figure 10 for more complex (possibly nematic elastomer) transformations.*

2.2. **Iteration of layers.** Next, motivated by experimentally observed nested structures ("tripole star structures", see Section 2.4), by the symmetry considerations from Corollary 2.4 and by the wish to consider the passage $n \to \infty$ (see Section 4), we seek to iterate the construction from Section 2.1 (as illustrated in Figure 4) leading to several nested "onion ring layers" of the described deformations. Imagining a nucleation mechanism starting from a single layer and gradually enlarging the volume fraction of the martensite this seems to be a natural construction. From the literature on the geometrically linearised theory of tripole star structures (see for instance [CPL14] and the appendix in [RZZ19]) and by virtue of the symmetry

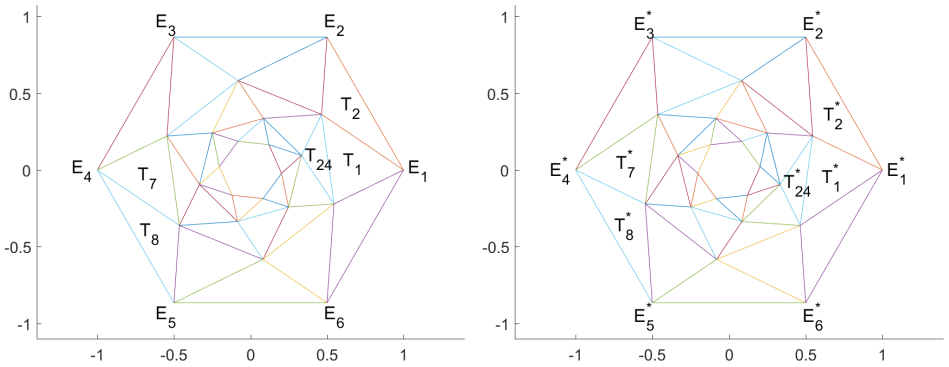

(A) (B)

FIGURE 4. Nested $n-$gons with $n = 6$. On the left and on the right, respectively before and after the action of u. Here, we denoted by E_i^*, T_i^* the quantities $u(E_i), u(T_i)$. Corollary 2.4 below states that ∇u is the same in T_1, T_7 and in T_{24}, where we denoted by T_{24} the triangle $T_{24} = r_I Q_\alpha T_{12} = r_I Q_\alpha Q_{-1} T_2$.

result of Corollary 2.4, one initially might hope that an iteration of the individual layers is possible without incurring stresses. As one of the main results of this section, we however show that if only finitely many wells are present, such an iteration of onion ring layers necessarily leads to the *presence* of (small) stresses in the geometrically non-linear theory. This mirrors the experimentalists' view who describe these constructions as disclinations [KK91].

We begin our discussion of the iterated onion ring structures by fixing notation. To this end, recall the notation from Section 2.1.2 and the compatibility conditions from Theorem 1. With these in hand, we now

- fix $\alpha > 0$,
- set for a matter of simplicity $r_E = 1$,
- and take r_I satisfying (15).

Further we introduce the following convention on the notation for rotations which we will frequently use here and in the sequel:

$$Q_\varphi := Q(\frac{2\pi}{n}\varphi) \text{ with } Q(\varphi) := \begin{pmatrix} \cos(\varphi) & -\sin(\varphi) \\ \sin(\varphi) & \cos(\varphi) \end{pmatrix} \in SO(2). \tag{20}$$

Let now u satisfying (i)–(iv) be given by the explicit single layer construction from Theorem 1 (ii) (see the proof in Section 3.1.2 for the details of this). Without loss of generality, by possibly premultiplying with a fixed rotation, below we consider $v_n = R_E u_n$, where as in the proof of Theorem 1 (ii), R_E is such that $\nabla v_n|_{T_1} = H$, and H is as in (17) (cf. proof of Theorem 1 (ii) in Section 3.1.2). In particular, the rotation in the interior $n-$gon of the first onion ring is given by $R_E R_*$ where R_* is as in (iv). We thus concatenate the first onion ring layer with a second, by r_I rescaled and by $Q_{-\alpha}$ rotated onion ring layer with exterior rotation $R_E R_*$. Iterating this N_n times yields a deformation v_n which is defined by the expression

$$\begin{aligned} v_n(x) = &\sum_{k=0}^{N_n} r_I^k R_E R_*^k Q_\alpha^k u(r_I^{-k} Q_{-\alpha}^k x) \chi_{\Sigma_k}(x) \\ &+ R_E x \chi_{\mathbb{R}^2 \setminus \Sigma_0^{co}}(x) + R_E R_*^{N_n+1} x \chi_{\overline{\Sigma}_{N_n+1}^{co}}(x), \end{aligned} \tag{21}$$

where χ_B is the indicator function on the set B, Q_α is a rotation of angle $\frac{2\pi}{n}\alpha$ and the sets Σ_i are defined by

$$\Sigma_i := \{x \in \mathbb{R}^2 : |x| \in r_I^i Q_\alpha^i \Omega_n\}.$$

We added a subscript n to v in order to highlight that r_I as much as R_* and u depend on n. We emphasise that in addition to the n-dependence, the only other parameter that v_n depends on is given by α. For simplicity, the positive integer N_n is chosen such that $N_n := \inf\{N \in \mathbb{N} : r_I^N \leq \frac{1}{2}\}$.

We now seek to understand the properties of these iterated deformations. In particular, a priori, it is not obvious that the deformation v_n satisfies the same differential inclusion

$$\nabla v_n(x) \in \bigcup_{P\in\mathcal{P}_n} SO(2)PHP^T = \bigcup_{P\in\mathcal{P}_n} SO(2)PUP^T \tag{22}$$

as the deformation gradient ∇u from the individual layers (as constructed in Theorem 1 (ii)) and with $\mathcal{P}_n$ as in (12). If the inclusion (22) were to hold, it would imply that v_n corresponds to an *exactly stress-free* deformation associated with a phase transformation with associated symmetry group $\mathcal{P}_n$. However, it will turn out that while (22) is true on each individual "onion ring layer" for some suitable U, it is no longer true for the overall concatenated construction.

Recalling our definition of v_n, in Cartesian coordinates the validity of the iterability of our construction boils down to the question whether

$$R_* Q_\alpha \nabla u Q_{-\alpha} \in \bigcup_{P\in\mathcal{P}_n} SO(2)PUP^T. \tag{23}$$

In the following we show that this condition *can not* be exactly satisfied with our choice of symmetry group $\mathcal{P}_n$ unless $\alpha = \frac{1}{2}$, in which case the construction is trivial. More precisely, we show that for $\alpha \neq \frac{1}{2}$, the inclusion (23) can only hold for either the outer *or* the inner triangles of the iterated ring:

Proposition 2.6. *Recall that the deformation v_n from (21) only depends on the parameters $n \in \mathbb{N}$, $\alpha \in (0,1)$. Then, for any $\alpha \in (0,1) \setminus \{\frac{1}{2}\}$ and any n fixed there exists a level set of the gradient of v_n in the first iterated ring such that*

$$\nabla v_n(x) = R_* Q_\alpha \nabla u Q_{-\alpha} \notin \bigcup_{P\in\mathcal{P}_n} SO(2)PUP^T. \tag{24}$$

Moreover, the inclusion (23) holds for the outer triangles of the inner onion ring but not for the inner ring.

Thus, any nucleation mechanism involving multiple layers of the individually stress-free onion ring constructions necessarily leads to the presence of stresses (we refer to Section 2.4 for some energetic back-of-the envelope calculations on their size).

2.3. **The geometrically linearised situation.** After having discussed the geometrically non-linear construction involving finitely many wells, we turn to its geometrically linearised counterpart. Here as our main result we infer that the geometrically linearised version of the single layer constructions only involve n different strain matrices (instead of the possibly $2n$ in the geometrically non-linear setting) and that the constructions can be iterated *without* incurring stresses.

In order to linearise the non-linear problem, we assume that $\alpha \sim \frac{1}{2}$ and define our (iterated) linearised infinitesimal deformations as $\tilde{v}_n(x) := \frac{d}{d\alpha} v_{n,\alpha}(x)|_{\alpha=\frac{1}{2}}$. Here $v_{n,\alpha}(x)$ denotes the deformation from (21), where we have added the angular dependence in the subscript for clarity.

Theorem 2. *Let $v_{n,\alpha} : \Omega_n \to \mathbb{R}^2$ denote the deformations constructed in Section 2.2 (for $\alpha \in (0,1)$). Then, the deformations $\tilde{v}_n(x) := \frac{d}{d\alpha} v_{n,\alpha}(x)|_{\alpha=\frac{1}{2}}$ are exactly stress-free deformations which attain only n values for their symmetrised deformation gradients which are all related by the action of the symmetry group. In other words, for almost every $x \in \Omega_n$*

$$e(\nabla \tilde{v}_n)(x) \in \{E_1, \dots, E_n\} := \left\{ Q_j E_1 Q_j^T : \ j \in \{0, \dots, n-1\} \right\},$$

where

$$E_1 = \frac{d}{d\alpha}[e(U_1(\alpha))]|_{\alpha=\frac{1}{2}} = \begin{pmatrix} 1 & -\frac{\cos(\phi_n/2)}{\sin(\phi_n/2)} \\ -\frac{\cos(\phi_n/2)}{\sin(\phi_n/2)} & -1 \end{pmatrix},$$

and where we use the notation $Q_j := Q\left(\frac{2\pi}{n} j\right)$. Moreover, the following symmetry assertions hold true:

(i) If $n = 2k+1$, $k \in \mathbb{N}$, we have for all $j \in \{1, \dots, n\}$

$$Q_{\frac{n-1}{2}} P_0 E_j P_0 Q_{\frac{n-1}{2}}^T = E_j,$$

and if $n = 2k$, $k \in \mathbb{N}$, we have for all $j \in \{1, \dots, n\}$

$$Q_{\frac{n}{2}} E_j Q_{\frac{n}{2}}^T = E_j.$$

(ii) For all $j \in \{1, \dots, n\}$ we have

$$R_{\frac{1}{2}} E_{j-1} R_{-\frac{1}{2}} = Q_1 E_j Q_1^T.$$

Let us discuss the implications of this result:

- While in the geometrically non-linear setting already in the case of a single onion ring layer, it is necessary to work with a phase transformation with $2n$ wells if n is odd (but only n wells is n is even), in the geometrically linearised case (linearised at $\alpha = \frac{1}{2}$) only n wells are needed, independently of whether n is odd or even (see Section 3.3.1). This leads to extremely symmetric "nested", geometrically refining constructions which, for instance, closely resemble the tripole star deformations (see Section 2.4). In this sense, the *geometry* of low energy solution is well-captured by the linearised theory.
- In contrast to the geometrically non-linear setting, the geometrically linearised solutions (at $\alpha = \frac{1}{2}$) *can* be iterated into solutions involving only n variants of martensite *without* incurring stresses. As already noted in the materials science literature the presence of "disclinations" [KK91] hence is a purely *geometrically non-linear* effect (see Section 3.3.2). Thus, while capturing the overall geometry of, for instance, the tripole star structures well, the geometrically linearised theory does *not* reflect the energetics of these deformations correctly. For a finer (energetic) analysis of the properties of these nucleation mechanisms it is thus necessary to work in the framework of the geometrically non-linear theory.

2.4. **Discussion of our results for the tripole star deformation.** We conclude our discussion of the "Conti-type constructions" for finite n by reconsidering an experimentally observed structure which gives evidence of the relevance of our proposed constructions. For $\alpha \approx 1/2$, $n = 3$ our solutions from Theorem 1 (ii) display self-similar "nested" structures as in Figure 5 (see also Corollary 2.4 which "explains" this symmetry). These are reminiscent of "tripole star structures" – a distinctive type of patterns which are observed in a class of metal alloys undergoing the (three-dimensional) hexagonal-to-orthorhombic transition in the plane [MA80a, MA80b, KKK88, KK91], a transformation characterised by three martensitic variants with special rotational symmetries. Investigation of these

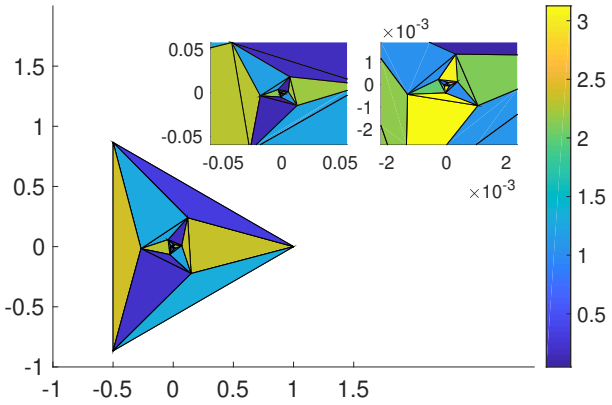

FIGURE 5. Exact construction of a self-similar tripole star obtained by solving (19). Here we set $\alpha = 0.47$. The colour map represents the eigenvector associated with the largest eigenvalue of the right Cauchy–Green tensor $\nabla u^T \nabla u$ which is parametrised as $(\cos\theta, \sin\theta, 0)$, we refer to the end of Section 4.1 for more information on the numerics producing these figures. The right tensor is rotated by an angle equal to $\frac{2\pi}{3}\alpha$ when moving across each hierarchy in the onion construction. Each layer consists of a sharp $\frac{\pi}{3}$ rotation dictated by the symmetry of the problem and an additional small rotation of amplitude equal to $\frac{\pi}{3}|1-2\alpha|$ which is required by compatibility and which causes additional rotational stretch (see in-plot magnifications).

types of microstructures (typically in two-dimensional models of the hexagonal-to-orthorhombic transformation) has been an object of extensive numerical studies based on the minimisation of stored energies defined in both fully non-linear and linearised elasticity for the hexagonal-to-orthorhombic transformation (see, for instance [CKO+07, WWC99, JCD04, CJ01, PL13] and the references quoted therein). Ultimately, in many of these works minimisation boils down to solving the associated differential inclusion problem (of the form (3)), for a piecewise affine vector $u : \Omega \to \mathbb{R}^2$ to be taken over a domain Ω and with boundary conditions that are suitable to reproduce the tripole stars.

In the experimental literature on the hexagonal-to-orthorhombic phase transformation, it is noted that the observed star patterns are of low but not of vanishing energy, in the sense that they are not exactly stress-free within the geometrically non-linear theory of elasticity. The experimental literature describes these structures as disclinations. This is in accordance with our results from the previous sections stating that

(i) a single, exactly stress-free layer of a tripole star deformation can not be achieved with three variants of martensite, but requires six variants,
(ii) an iteration of the individual layers is not possible with only three (or six) variants of martensite. Already in the second layer, this will lead to misfits (which give rise to the experimentally observed stresses). In [VD76], for instance, the authors report a deviation of the outer-most and the second inner iteration by roughly four degrees.

As also observed in the literature [KK91] (and also confirmed by our analysis, see Section 2.3) this is a *geometrically non-linear* effect. Indeed, by introducing the geometrically linearised elasticity version of the (two-dimensional) hexagonal-to-orthorhombic phase transformation, an exact construction of a self-similar tripole star pattern has been obtained in [CPL14] by imposing kinematic compatibility across each interface and by defining a displacement field that reproduces the three martensitic variants associated with the hexagonal-to-orthorhombic transformation. The symmetry and rigidity of the problem is inherited in the shape of the microstructure in that the tripole stars are obtained by rotating, rescaling and translating a copy of a single kite-shaped polygon which is perfectly symmetric with respect to its axes.

The results of Section 2.1 generalise the linearised construction of [CPL14] in the following way. By replacing the non-linear differential inclusion associated with the hexagonal-to-orthorhombic transformation with (19) which involves extra rotations (and reflections) of the bain strain matrices and therefore more flexibility, it is possible to construct exact tripole stars by matching rotated and dilated copies of slightly non-symmetrical tetrahedra and to quantify the deviation from the perfectly symmetric construction of the linearised case. Thanks to (18) we can estimate from above the nonlinear elastic mismatch in one single layer of our construction caused by having just three martensitic variants (hexagonal-to-orthorhombic transformation) rather than six (as in [CKZ17] or Theorem 1 (ii)). Indeed, using the symmetry from Corollary 2.4 this can be bounded from above by (cf. Section 3.3.1)

$$|H - H^T| = \tan\Big(\frac{\pi}{3}\Big)|a - a^{-1}|,$$

and so is small whenever $a \approx 1$. As the results of Section 2.3 show, this small mismatch is *not* captured by the linear elasticity model.

In order to achieve the matching across every annulus, the deformation field necessarily has to incorporate, at each hierarchy, an additional rotation Q_α of an angle equal to $\frac{2\pi}{3}\alpha$ (see also the comment in the caption of Figure 5). This leads to the presence of elastic energies.

Indeed, it is interesting to view the constructions from an energetic point of view. Setting $K_3(a) := \bigcup_{P\in\mathcal{P}_3} SO(2)PH(a)P^T$ with $H(a)$ as in (17), we consider the energy

$$\mathcal{E}_3(\nabla u) = \int_{\Omega_3} \operatorname{dist}^2(\nabla u, K_3(a)\cup SO(2))dx + \epsilon|\nabla^2 u|(\Omega_3).$$

Here the additional well $SO(2)$ corresponds to the austenite phase. For this energy, the *single layer* deformations from Theorem 1 (ii) are extremely inexpensive: the elastic energy vanishes, while the surface energy is finite. Hence the energy behaves like $C\epsilon$ for some constant $C > 0$. However, *iterated* constructions as in Proposition 4.1 already cost more: here, by the geometric refinement of the structures, the surface energy still behaves as $C\epsilon$ for some constant $C > 0$, while the elastic energy can be estimated by

$$E_{elast} \leq C\sum_{j=1}^{N_3} r_I^{2j} \operatorname{dist}^2(Q_{\alpha j}^T \nabla u^T \nabla u Q_{\alpha j}, \bigcup_{j=1}^{6} H_j^T H_j),$$

where $H_j = Q_{\frac{j-1}{2}} H(a)^T H(a) Q_{\frac{j-1}{2}}^T$ if j is odd and $H_j = Q_{\frac{j-2}{2}} H(a)^T H(a) Q_{\frac{j-2}{2}}^T$ if j is even and $H(a)$ is as in (17). By arguments as in the proof of Proposition 2.6 for

α close to $\frac{1}{2}$ and $N_3 \in \mathbb{N}$ not too large, the total energy thus is controlled by

$$\mathcal{E}_3(\nabla v_3) \leq C \sum_{j=1}^{N_3} r_I^{2j} \operatorname{dist}^2(2j\alpha, \mathbb{Z}) + C\epsilon.$$

Hence, we obtain a three parameter minimisation problem, with the parameters α, ϵ, N_3 (where the N_3 dependence is mild as the series in j is summable as a geometric series). In particular, in spite of the presence of stresses, for $\alpha \in (0,1)$ sufficiently close to $\frac{1}{2}$ (depending on N_3 and ϵ) there is a regime, in which also in the geometrically non-linear setting, it is feasible that the tripole star structures are observed and are rather stable.

3. Proofs for the Constructions for Finite N

In this section, we present the proofs of the results from Section 2. We begin by explaining the proofs of the necessary and sufficient conditions in Section 3.1, then provide the arguments for the iterability results in Section 3.2 and finally conclude with the analysis of the geometrically linearised setting in Section 3.3.

3.1. Proof of the necessary and sufficient conditions.

We begin with the proof of the necessary and sufficient conditions for the nucleation mechanism involving a geometrically non-linear Conti-type single layer construction.

Before turning to the proofs of the individual results, we make the following observation allowing us to deal with products of rotations and reflections:

Remark 3.1. *In the sequel, we will often rely on the following commutation relations: Given $U \in \mathbb{R}^{2\times 2}$, and any $Q \in SO(2)$, then*

$$\bigcup_{P\in\mathcal{P}_n} SO(2)PQUP^T = \bigcup_{P\in\mathcal{P}_n} SO(2)PUP^T.$$

Indeed, if $P \in \mathcal{R}_1^n$, then $QP = PQ$. If instead $P \in \mathcal{R}_2^n$, then $PQ = Q^T P$.

Remark 3.2. *In view of Remark 3.1, we can replace the symmetric matrix $U = U(a)$ in (14) equivalently by any matrix of the form RU with $R \in SO(2)$. We will therefore from now on work mostly with the (simpler) matrix $H = H(a)$ given in (17).*

3.1.1. *The necessary conditions.*

In deducing the necessary conditions for the existence of the described nucleation mechanism (i.e. in proving (13)–(14)) we argue along the lines of [CKZ17], which we present for self-containedness.

Proof of Theorem 1 (i). Let us start by noticing that, since we assume that for each $i = 1, \dots, n$ the deformation u is affine in T_i, then $\nabla u|_{T_i} = F_i$, for some $F_i \in \mathbb{R}^{2\times 2}$.

As in [CKZ17], we now first identify suitable eigenvectors and eigenvalues in the construction: Let $l_1 = |\overline{I_{i-1}E_i}|$ and $l_2 = |\overline{I_iE_i}|$ for $i = 1, \dots, n$ (where we remark that by symmetry these lengths are independent of $i \in \{1, \dots, n\}$, c.f. Definition 2.1). By (iv), i.e. by the "flipping" of the internal points of the outer triangles, there exist $v_{n1}, v_{11} \in \mathbb{S}^1$ such that

$$F_1\overline{I_nE_1} = F_1 l_1 e_{n1} = l_2 v_{n1}, \qquad F_1\overline{I_1E_1} = F_1 l_2 e_{11} = l_1 v_{11},$$

and a rotation $\hat{R} \in SO(2)$ such that

$$\hat{R}e_{n1} = v_{n1}, \qquad \hat{R}e_{11} = v_{11},$$

see also Figures 2-6. Therefore,

$$e_{n1} \cdot e_{11} = \hat{R}e_{n1} \cdot \hat{R}e_{11} = v_{n1} \cdot v_{11},$$

and, setting $R := \hat{R}^T$,

$$RF_1 e_{n1} = \frac{1}{a} e_{n1}, \qquad RF_1 e_{11} = a e_{11}, \tag{25}$$

where $a := \frac{l_1}{l_2}$. Since u is continuous, it must hold that

$$RF_2 e_{11} = a e_{11}. \tag{26}$$

Furthermore, repeating the above arguments based on the condition (iv) (which simply follows by symmetry as T_3 is a rotation of T_1 by $\frac{2\pi}{n}$), we have that

$$RF_3 e_{12} = \frac{1}{a} e_{12}, \qquad RF_3 e_{22} = a e_{22}.$$

The continuity of u then again implies that

$$RF_2 e_{12} = \frac{1}{a} e_{12}. \tag{27}$$

Let us suppose now that there exists $P, Q \in O(2)$ with $\det P \det Q = 1$ such that $RF_1 = PRF_2Q$. Then,

$$\begin{aligned} a &= a|P^T e_{11}| = |P^T RF_1 e_{11}| = |RF_2 Q e_{11}|, \\ \frac{1}{a} &= \frac{1}{a}|P^T e_{n1}| = |P^T RF_1 e_{n1}| = |RF_2 Q e_{n1}|. \end{aligned}$$

But, by (26)–(27), a and $\frac{1}{a}$ are simple eigenvalues of RF_2 and thus $Qe_{11} = \pm e_{11}$ and $Qe_{n1} = \pm e_{12}$. Hence,

$$\cos\phi := e_{11} \cdot e_{n1} = Qe_{11} \cdot Qe_{n1} = \pm e_{11} \cdot e_{12} = \pm \cos\Big(\frac{2\pi}{n} + \phi\Big).$$

The only solution ϕ to this equation in the interval $\Big(0, \frac{\pi(n-2)}{n}\Big)$ (where the construction is respected) is $\phi = \frac{\pi(n-2)}{2n}$. Furthermore, defining $H := RF_1$, by (25), it must be of the form

$$H = RF_1 = a e_{11} \otimes e_{11} + \frac{1}{a} e_{11}^{\perp} \otimes e_{11}^{\perp} + \frac{a^{-1} - a}{\tan\phi} e_{11} \otimes e_{11}^{\perp}, \tag{28}$$

where $e_{11}^{\perp}$ is such that $e_{11} \times e_{11}^{\perp} > 0$ and where we exploited the fact that $e_{n1} = \cos(\phi) e_{11} + \sin(\phi) e_{11}^{\perp}$. This concludes the argument for (13) and (14) in view of Remarks 2.3 and 3.2.

The statement on the symmetry group then follows from the symmetry of the domains.

We next discuss the derivation of the identities (15) and (16). In order to prove (15), we first notice that on the one hand,

$$l_1 = |E_1 - I_n| = \sqrt{r_E^2 + r_I^2 - 2 r_E r_I \cos\Big(\frac{2\pi}{n}(1-\alpha)\Big)}, \tag{29}$$

$$l_2 = |E_1 - I_1| = \sqrt{r_E^2 + r_I^2 - 2 r_E r_I \cos\Big(\frac{2\pi}{n}\alpha\Big)}. \tag{30}$$

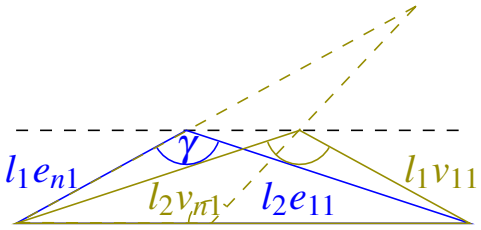

FIGURE 6. An illustration of the eigenvalue condition identified in the proof of Proposition 1. We observe that $e_{n1} \cdot e_{11} = v_{n1} \cdot v_{11} = \cos(\gamma)$ and that there exists $\hat{R} \in SO(2)$ such that $\hat{R}e_{n1} = v_{n1}$ and $\hat{R}e_{11} = v_{11}$. After a rotation the image triangle (in green) can be rotated onto the reference triangle (in blue). This yields the triangle whose sides are depicted with the green dashed lines. Formalising this leads to the proof of (25).

On the other hand,

$$
\begin{aligned}
l_1 l_2 \cos\phi &= \overline{E_1 I_n} \cdot \overline{E_1 I_1} = (I_n - E_1) \cdot (I_1 - E_1) \\
&= \begin{pmatrix} r_I \cos(\frac{2\pi}{n}(\alpha-1)) - r_E \\ r_I \sin(\frac{2\pi}{n}(\alpha-1)) \end{pmatrix} \cdot \begin{pmatrix} r_I \cos(\frac{2\pi}{n}\alpha) - r_E \\ r_I \sin(\frac{2\pi}{n}\alpha) \end{pmatrix} \\
&= r_E^2 + r_I^2 \left(\cos(\frac{2\pi}{n}\alpha)\cos(\frac{2\pi}{n}(\alpha-1)) + \sin(\frac{2\pi}{n}\alpha)\sin(\frac{2\pi}{n}(\alpha-1)) \right) \\
&\quad - r_I r_E \left(\cos(\frac{2\pi}{n}(\alpha-1)) + \cos(\frac{2\pi}{n}\alpha) \right) \\
&= r_E^2 + r_I^2 \cos(\frac{2\pi}{n}) - r_I r_E \left(\cos(\frac{2\pi}{n}(\alpha-1)) + \cos(\frac{2\pi}{n}\alpha) \right) \\
&= r_E^2 + r_I^2 \cos\Big(\frac{2\pi}{n}\Big) - 2 r_I r_E \cos\Big(\frac{\pi}{n}(2\alpha-1)\Big)\cos\Big(\frac{\pi}{n}\Big).
\end{aligned} \tag{31}
$$

Here, in the last step, we have used the trigonometric identity

$$
\cos(\psi_1) + \cos(\psi_2) = 2\cos\left(\frac{1}{2}(\psi_1+\psi_2)\right)\cos\left(\frac{1}{2}(\psi_1-\psi_2)\right).
$$

Taking the square of (31) and exploiting (29)–(30) gives a fourth order equation in $x = \frac{r_I}{r_E}$. Out of the four solutions of this equation, the only satisfying (31) and such that $x \in (0,1)$ provided $\alpha \in (0,1)$ is given by (15). We refer the reader to Appendix A for the details. Furthermore, using that $a = \frac{l_1}{l_2}$ and exploiting (15) in (29)–(30) we deduce (16). □

3.1.2. *The sufficient conditions.* We discuss the sufficiency of the necessary condition by explicitly and systematically constructing a "single layer" Conti construction, which will be a deformation as illustrated in Figure 3.

Proof of Theorem 1 (ii). We argue in three steps. Here we first construct a tensor field F in $\Omega_n^E \setminus \Omega_n^I$, and then in $\mathbb{R}^2 \setminus \Omega_n^E$ and Ω_n^I. Finally, we discuss the overall compatibility, showing that $F = \nabla u$ for some piecewise constant deformation $u : \mathbb{R}^2 \to \mathbb{R}^2$.

Step 1: Deformation in the region $\Omega_n^E \setminus \Omega_n^I$. We first construct a piecewise constant tensor field $F : \Omega_n^E \setminus \Omega_n^I \to \mathbb{R}^{2\times 2}$. Let us start by setting $F = H$ in T_1, and $F = P_0 H P_0$ in T_2, where $P_0 = e_{11} \otimes e_{11} - e_{11}^\perp \otimes e_{11}^\perp \in O(2)$. We have that H

and P_0HP_0 are compatible across the line parallel to e_{11}. Indeed,

$$H - P_0HP_0 = 2\frac{a^{-1}-a}{\tan\phi}e_{11}\otimes e_{11}^{\perp}, \qquad \big(H-P_0HP_0\big)e_{11}=0. \tag{32}$$

Then, we define F as follows:

$$F = \begin{cases} Q_{\frac{j-1}{2}}HQ_{\frac{j-1}{2}}^T, & \text{in } T_j \text{ if } j \text{ odd},\\ Q_{\frac{j-2}{2}}P_0HP_0Q_{\frac{j-2}{2}}^T, & \text{in } T_j \text{ if } j \text{ even}. \end{cases} \tag{33}$$

Here $Q_\varphi := Q(\frac{2\pi}{n}\varphi)$ with $Q(\varphi) := \begin{pmatrix}\cos(\varphi) & -\sin(\varphi)\\ \sin(\varphi) & \cos(\varphi)\end{pmatrix} \in SO(2)$. Furthermore, we have

$$\begin{aligned} e_{n1} &= \cos(\phi)e_{11}+\sin(\phi)e_{11}^{\perp} = \sin\Big(\frac{\pi}{n}\Big)e_{11}+\cos\Big(\frac{\pi}{n}\Big)e_{11}^{\perp},\\ e_{12} &= \cos\Big(\phi+\frac{2\pi}{n}\Big)e_{11}+\sin\Big(\phi+\frac{2\pi}{n}\Big)e_{11}^{\perp} = -\sin\Big(\frac{\pi}{n}\Big)e_{11}+\cos\Big(\frac{\pi}{n}\Big)e_{11}^{\perp}, \end{aligned} \tag{34}$$

so that $P_0e_{12} = -e_{n1}$. This yields,

$$\begin{aligned} F|_{T_2}e_{12} &\overset{(33)}{=} P_0HP_0e_{12} = -P_0He_{n1} \overset{(17)}{=} -\frac{1}{a}P_0e_{n1} = \frac{1}{a}e_{12}\\ &= Q_1He_{n1} = Q_1HQ_1^Te_{12} \overset{(33)}{=} F|_{T_3}e_{12}, \end{aligned}$$

and hence

$$F|_{T_2} - F|_{T_3} = c\otimes e_{12}, \tag{35}$$

for some $c\in\mathbb{R}^2$. Now, using that $e_{i,i+1} = Q_1e_{i-1,i}$ and that $e_{i+1,i+1} = Q_1e_{i,i}$, by (32)–(35), we obtain

$$\big(F|_{T_i} - F|_{T_{i+1}}\big)e_{ii} = 0, \qquad \text{if } i \text{ odd}, \tag{36}$$

$$\big(F|_{T_i} - F|_{T_{i+1}}\big)e_{i,i+1} = 0, \qquad \text{if } i \text{ even}, \tag{37}$$

again using the convention that $n+1=1$ and $0=n$.

Step 2: Construction of the deformation in $\mathbb{R}^2\setminus\Omega_n^E$ and Ω_n^I. We next extend F to be defined also in Ω_n^I and in $\mathbb{R}^2\setminus\Omega_n^E$. By construction (and in particular by the condition (iv) which just corresponded to the "flipping"/ "rotation" of the inner points), we have that $H\overline{I_nI_1} = R_I\overline{I_nI_1}$ for some $R_I\in SO(2)$. Therefore, H and R_I are compatible across the line parallel to $\overline{I_nI_1}$, that is

$$H - R_I = b\otimes\overline{I_nI_1}^{\perp},$$

for some $b\in\mathbb{R}^2$. As a consequence,

$$F|_{T_{2i-1}} = Q_{i-1}HQ_{i-1}^T = R_I + Q_{i-1}b\otimes\overline{I_{i-1}I_i}^{\perp}, \qquad i=1,\dots,n. \tag{38}$$

We set $F|_{\Omega_n^I} := R_I$.

We claim that similarly it is possible to deduce the existence of $R_E\in SO(2)$ and $v\in\mathbb{R}^2$ such that

$$F|_{T_{2i}} = R_E + Q_{i-1}v\otimes\overline{E_iE_{i+1}}^{\perp}, \qquad i=1,\dots,n. \tag{39}$$

To infer this, we observe the following: On the one hand, using the projection of e_{12} onto the basis $\{e_{11},e_{11}^{\perp}\}$ (see (34)) we obtain

$$|\overline{E_iE_{i+1}}|^2 = |l_2e_{11}-l_1e_{12}|^2 = l_2^2|e_{11}-ae_{12}|^2 = l_2^2\Big(1+a^2+2a\sin\Big(\frac{\pi}{n}\Big)\Big). \tag{40}$$

On the other hand, using (34) again, we have

$$|P_0HP_0(l_2e_{11}-l_1e_{12})|^2 = l_2^2\left|\left(a+\sin\left(\frac{\pi}{n}\right)\right)e_{11}-\cos\left(\frac{\pi}{n}\right)e_{11}^{\perp}\right|^2 = l_2^2\left(1+a^2+2a\sin\left(\frac{\pi}{n}\right)\right). \tag{41}$$

Combining both observations, we deduce the claim in (39) and define $F|_{\mathbb{R}^2\setminus\Omega_n^E} := R_E$.

Step 3: Overall compatibility and conclusion. Since the constructed tensor field $F:\mathbb{R}^2\to\mathbb{R}^{2\times 2}$ is piecewise constant and (36)–(39) hold, we have that $\nabla\times F=0$. Therefore, the fact that $\mathbb{R}^2$ is simply connected and [GR86, Thm. 2.9], imply the existence of a deformation $u\in W^{1,\infty}_{loc}(\mathbb{R}^2;\mathbb{R}^2)$ such that $F=\nabla u$ and such that $R_E^T u$ satisfies the conditions (i)–(iv). □

3.2. **Proofs of the iterability results.** In this section, we present the proofs of the iterability results stated in Section 2.2.

3.2.1. *Symmetry, proof of Corollary 2.4.* We begin by discussing the proof of Corollary 2.4, i.e. of the symmetry result of the deformation constructed in Theorem 1. This follows from analysing our explicit construction which was given in Section 3.1.2. We recall the convention on rotations from (20).

Proof of Corollary 2.4. In order to prove (18), we notice that, if n is even, $Q_{\frac{n}{2}}$ is a rotation by π, and therefore by (33) the claim follows. Let us hence assume that n is odd. By symmetry we can prove the claim by assuming $i=1$, that is we need to prove that

$$Q_{\frac{n-1}{2}}P_0HP_0Q_{\frac{n-1}{2}}^T = H^T. \tag{42}$$

But, using that $Q_{\frac{n-1}{2}} = -Q_{\frac{1}{2}}^T$,

$$Q_{\frac{n-1}{2}}P_0HP_0Q_{\frac{n-1}{2}}^T = Q_{\frac{1}{2}}^T\big(ae_{11}\otimes e_{11}+a^{-1}e_{11}^{\perp}\otimes e_{11}^{\perp}-\tan\frac{\pi}{n}(a^{-1}-a)e_{11}\otimes e_{11}^{\perp}\big)Q_{\frac{1}{2}},$$

and exploiting the fact that

$$Q_{\frac{1}{2}}^Te_{11} = \cos\left(\frac{\pi}{n}\right)e_{11}-\sin\left(\frac{\pi}{n}\right)e_{11}^{\perp}, \qquad Q_{\frac{1}{2}}^Te_{11}^{\perp} = \cos\left(\frac{\pi}{n}\right)e_{11}^{\perp}+\sin\left(\frac{\pi}{n}\right)e_{11},$$

we deduce (42).

In order to prove (19), we can again assume without loss of generality that $i=1$. Then, proving the statement reduces to showing that

$$R_*Q_\alpha P_0HP_0Q_\alpha^T = Q_1HQ_1^T,$$

or, equivalently, that

$$P_0HP_0 = Q_\alpha HQ_{1-\alpha}^T. \tag{43}$$

A proof of this equality is given in Appendix B; we also refer to the result and argument of the next proposition. □

3.2.2. *Proof of Proposition 2.6.* In this section we present the proof of the iteration of the single layer results. We show that while Corollary 2.4 implies that the inclusion (22) holds for the outer triangles of the inner onion ring, this fails for the inner triangles of the onion ring. Our argument also provides a second proof of the symmetry result from (19).

Proof of Proposition 2.6. We note that the inclusion problem (24) can be equivalently phrased in terms of the Cauchy-Green tensors. A self-contained proof of this reduction is provided in Lemma C.1. Using the explicit structure of ∇u given in equation (33) and that $R_j \in \mathcal{R}_1^n \subset \mathcal{P}_n$, it thus suffices to consider two triangles T_0, T_1 and the inclusion problems

$$\begin{aligned} Q_\alpha H^T H Q_{-\alpha} &\in \bigcup_{P\in\mathcal{P}_n} P^T H^T H P, \\ Q_\alpha P_0 H^T H P_0 Q_{-\alpha} &\in \bigcup_{P\in\mathcal{P}_n} P^T H^T H P, \end{aligned} \tag{44}$$

where

$$P_0 = P_0^T = \begin{pmatrix} e_{11} & e_{11}^\perp \end{pmatrix} \begin{pmatrix} 1 & 0 \\ 0 & -1 \end{pmatrix} \begin{pmatrix} e_{11} & e_{11}^\perp \end{pmatrix}^T \in O(2),$$

and

$$H = \begin{pmatrix} e_{11} & e_{11}^\perp \end{pmatrix} \begin{pmatrix} a & \frac{a^{-1}-a}{\tan(\phi)} \\ 0 & \frac{1}{a} \end{pmatrix} \begin{pmatrix} e_{11} & e_{11}^\perp \end{pmatrix}^T =: \begin{pmatrix} e_{11} & e_{11}^\perp \end{pmatrix} H_1 \begin{pmatrix} e_{11} & e_{11}^\perp \end{pmatrix}^T.$$

Furthermore, we may change our basis from the canonical unit basis to the basis $(e_{11}, e_{11}^\perp)$ and equivalently express (44) as

$$Q_\alpha H_1^T H_1 Q_{-\alpha} \in \bigcup_{P\in\hat{\mathcal{P}}_n} P^T H_1^T H_1 P, \tag{45}$$

$$Q_\alpha \operatorname{diag}(1,-1) H_1^T H_1 \operatorname{diag}(1,-1) Q_{-\alpha} \in \bigcup_{P\in\hat{\mathcal{P}}_n} P^T H_1^T H_1 P, \tag{46}$$

where

$$\hat{\mathcal{P}}_n = \mathcal{R}_1^n \cup \begin{pmatrix} 1 & 0 \\ 0 & -1 \end{pmatrix} \mathcal{R}_1^n =: \hat{\mathcal{R}}_1^n \cup \hat{\mathcal{R}}_2^n \tag{47}$$

is the standard dihedral group. We note that

$$H_1^T H_1 = \begin{pmatrix} a^2 & \frac{1-a^2}{\tan(\phi)} \\ \frac{1-a^2}{\tan(\phi)} & \frac{1}{a^2} + \left(\frac{a^{-1}-a}{\tan(\phi)}\right)^2 \end{pmatrix}, \tag{48}$$

is a symmetric matrix with determinant one and eigenvalues λ, λ^{-1}, which are distinct if and only if $\alpha \neq \frac{1}{2}$. Thus, there exists a rotation R_φ such that

$$H_1^T H_1 = Q_{-\varphi} \operatorname{diag}(\lambda, \lambda^{-1}) Q_\varphi. \tag{49}$$

Expressing (45) and (46) with respect to this diagonal matrix, we thus obtain the requirement that $\operatorname{diag}(\lambda, \lambda^{-1}) = Q^T \operatorname{diag}(\lambda, \lambda^{-1}) Q$ for a suitable $Q = Q(P, \alpha, \varphi) \in O(2)$ of the structure given below. Since we assume that $\lambda \neq \lambda^{-1}$ it follows that Q has to map the eigenvectors v_1, v_2 of $H_1^T H_1$ to $\pm v_1, \pm v_2$ and thus (45) and (46) are satisfied if and only if there exist $P \in \hat{\mathcal{P}}_n$ such that:

$$Q_\varphi P Q_\alpha Q_{-\varphi} \in \{Id, -Id, \operatorname{diag}(1,-1), \operatorname{diag}(-1,1)\}, \tag{50}$$

$$Q_\varphi P Q_\alpha \operatorname{diag}(1,-1) Q_{-\varphi} \in \{Id, -Id, \operatorname{diag}(1,-1), \operatorname{diag}(-1,1)\}, \tag{51}$$

respectively. We first consider (50) and note that if $P = Q_j \in \hat{\mathcal{R}}_1^n$ with $j \in \{1, \dots, n\}$, the left-hand-side reduces to $Q_{j+\alpha} \in \{Id, -Id\}$, which is never satified since $\alpha \in (0,1)$. If instead $P = \operatorname{diag}(1,-1) Q_j$ for $j \in \{1, \dots, n\}$, then

$$\begin{aligned} Q_\varphi P Q_\alpha Q_{-\varphi} &= Q_\varphi \operatorname{diag}(1,-1) Q_{j+\alpha} Q_{-\varphi} \\ &= Q_{\varphi - \frac{j+\alpha}{2}} \operatorname{diag}(1,-1) Q_{-\varphi + \frac{j+\alpha}{2}} \in \{\operatorname{diag}(1,-1), \operatorname{diag}(-1,1)\}, \end{aligned} \tag{52}$$

if and only if

$$\begin{aligned} &\frac{2\pi}{n}\left(-\varphi+\frac{j+\alpha}{2}\right)\in\pi\mathbb{Z}\\ \Leftrightarrow\ & j+\alpha-2\varphi\in n\mathbb{Z}\Leftrightarrow\alpha-2\varphi\in\mathbb{Z}. \end{aligned} \tag{53}$$

We will later compute φ to show that this condition is satisfied iff $\alpha=\frac{1}{2}$. Before proceeding to this, let us however also consider the second inclusion (51). If $P=\operatorname{diag}(1,-1)Q_j\in\hat{\mathcal{R}}_n^1$ for some $j\in\{1,\dots,n\}$, the left-hand-side of (50) reduces to

$$Q_\varphi Q_{-j-\alpha}\operatorname{diag}(1,-1)\operatorname{diag}(1,-1)Q_{-\alpha}=Q_{-j-\alpha}\notin\{Id,-Id\}.$$

If instead $P=Q_j$ for some $j\in\{1,\dots,n\}$, we obtain

$$\begin{aligned} &Q_\varphi Q_{j+\alpha}\operatorname{diag}(1,-1)Q_{-\varphi}\\ &=Q_\varphi Q_{(j+\alpha)/2}\operatorname{diag}(1,-1)Q_{-(j+\alpha)/2}Q_{-\varphi}\in\{\operatorname{diag}(1,-1),\operatorname{diag}(-1,1)\}, \end{aligned} \tag{54}$$

if and only if

$$\begin{aligned} &\frac{2\pi}{n}\left(-\varphi-\frac{j+\alpha}{2}\right)\in\pi\mathbb{Z}\\ \Leftrightarrow\ & -j-\alpha-2\varphi\in n\mathbb{Z}\Leftrightarrow-\alpha-2\varphi\in\mathbb{Z}. \end{aligned} \tag{55}$$

In particular, considering the difference of (53) and (55), we observe that for both inclusions (53) and (55) to be satisfied it is necessary that $2\alpha\in\mathbb{Z}$ and thus $\alpha=\frac{1}{2}$. This concludes the proof of the first statement of the proposition.

We additionally show that (55) is always satisfied for all $\alpha\in(0,1)$ by computing $\varphi=\varphi(\alpha)$. Indeed, we claim that

$$v=\left(\cos\left(\frac{2\pi}{n}\frac{\alpha-1}{2}\right),\sin\left(\frac{2\pi}{n}\frac{\alpha-1}{2}\right)\right) \tag{56}$$

is an eigenvector of $H_1^TH_1$. Since φ was defined by $H_1^TH_1=Q_{-\varphi}\operatorname{diag}(\lambda,\lambda^{-1})Q_{-\varphi}^T$, this implies that $\varphi=-\frac{\alpha-1}{2}$ and hence (55) is satisfied. It remains to show that v is indeed an eigenvector. As we consider two-dimensional matrices, it suffices to show that $H_1^TH_1v$ is colinear to v and thus equivalently

$$\begin{aligned} 0&=v^T\begin{pmatrix}0&-1\\1&0\end{pmatrix}H_1^TH_1v\\ &=\left(\frac{1}{a^2}-a^2+\left(\frac{a^{-1}-a}{\tan(\phi)}\right)^2\right)\sin\left(\frac{2\pi}{n}\frac{\alpha-1}{2}\right)\cos\left(\frac{2\pi}{n}\frac{\alpha-1}{2}\right)\\ &\quad+\frac{1-a^2}{\tan(\phi)}\left(\cos^2\left(\frac{2\pi}{n}\frac{\alpha-1}{2}\right)-\sin^2\left(\frac{2\pi}{n}\frac{\alpha-1}{2}\right)\right)\\ &=\left(\frac{1}{a^2}-a^2+\left(\frac{a^{-1}-a}{\tan(\phi)}\right)^2\right)\frac{1}{2}\sin\left(\frac{2\pi}{n}(\alpha-1)\right)\\ &\quad+\frac{1-a^2}{\tan(\phi)}\cos\left(\frac{2\pi}{n}(\alpha-1)\right). \end{aligned} \tag{57}$$

We recall that by (16)

$$\begin{aligned} &a^2=\frac{\sin(\frac{2\pi}{n}(1-\alpha))}{\sin(\frac{2\pi}{n}\alpha)},\ \tan(\phi)=\tan\left(\frac{n-2}{2n}\pi\right)=\cot\left(\frac{\pi}{n}\right),\\ &(a^{-1}-a)^2=a^{-2}+a^2-2. \end{aligned}$$

We now note that the equality (57) is satisfied if $a^2 = 1$ and thus $\alpha = \frac{1}{2}$, otherwise we may divide by $(1 - a^2)$ to further reduce to proving

$$\left(a^{-2} + 1 + (a^{-2} - 1)\tan^2\left(\frac{\pi}{n}\right)\right)\frac{1}{2}\sin\left(\frac{2\pi}{n}(\alpha - 1)\right) + \cos\left(\frac{2\pi}{n}(\alpha - 1)\right)\tan\left(\frac{\pi}{n}\right) = 0.$$

For easier notation, we introduce $\gamma = \frac{2\pi}{n}\alpha$, $\beta = \frac{2\pi}{n}(\alpha - 1) = \gamma - \frac{2\pi}{n}$, and thus $a^{-2} = -\frac{\sin(\gamma)}{\sin(\beta)}$. Then the above simplifies to

$$\frac{1}{2}\left(-\sin(\gamma) + \sin(\beta) + (-\sin(\gamma) - \sin(\beta))\tan^2\left(\frac{\pi}{n}\right)\right) + \cos(\beta)\tan\left(\frac{\pi}{n}\right) = 0.$$

We then insert $\sin(\gamma) = \cos(\beta)\sin\left(\frac{2\pi}{n}\right) + \sin(\beta)\cos\left(\frac{2\pi}{n}\right)$ and collect terms involving $\cos(\beta)$ and $\sin(\beta)$:

$$\begin{aligned}\cos(\beta)&\left(-\frac{1}{2}\left(\sin\left(\frac{2\pi}{n}\right) + \sin\left(\frac{2\pi}{n}\right)\tan^2\left(\frac{\pi}{n}\right)\right) + \tan\left(\frac{\pi}{n}\right)\right)\\ +\sin(\beta)&\frac{1}{2}\left(-\cos\left(\frac{2\pi}{n}\right) + 1 - \left(\cos\left(\frac{2\pi}{n}\right) + 1\right)\tan^2\left(\frac{\pi}{n}\right)\right) = 0.\end{aligned}$$

In order to observe that this is indeed correct, we use the double-angle identities $\sin(\frac{2\pi}{n}) = 2\sin(\frac{\pi}{n})\cos(\frac{\pi}{n})$ and $\cos(\frac{2\pi}{n}) = \cos^2(\frac{\pi}{n}) - \sin^2(\frac{\pi}{n})$ to obtain that

$$\begin{aligned}&-\frac{1}{2}\left(\sin\left(\frac{2\pi}{n}\right) + \sin\left(\frac{2\pi}{n}\right)\tan^2\left(\frac{\pi}{n}\right)\right) + \tan\left(\frac{\pi}{n}\right)\\ &= -\left(\sin\left(\frac{\pi}{n}\right)\cos\left(\frac{\pi}{n}\right) + \sin\left(\frac{\pi}{n}\right)\cos\left(\frac{\pi}{n}\right)\left(\frac{1}{\cos^2\left(\frac{\pi}{n}\right)} - 1\right)\right) + \frac{\sin(\frac{\pi}{n})}{\cos(\frac{\pi}{n})} = 0,\end{aligned}$$

as well as

$$\begin{aligned}&-\cos\left(\frac{2\pi}{n}\right) + 1 - \left(\cos\left(\frac{2\pi}{n}\right) + 1\right)\tan^2\left(\frac{\pi}{n}\right)\\ &= -\cos^2\left(\frac{\pi}{n}\right) + \sin^2\left(\frac{\pi}{n}\right) + 1 - \left(\cos^2\left(\frac{\pi}{n}\right) - \sin^2\left(\frac{\pi}{n}\right) + 1\right)\tan^2\left(\frac{\pi}{n}\right)\\ &= 2\sin^2\left(\frac{\pi}{n}\right) - 2\cos^2\left(\frac{\pi}{n}\right)\tan^2\left(\frac{\pi}{n}\right) = 0.\end{aligned}$$

This concludes the proof. □

3.3. **Linearisation.** In this section, we provide the arguments leading to the proof of Theorem 2. To this end, we begin by deriving a geometrically linear Conti construction from the geometrically non-linear one by linearisation at $\alpha = \frac{1}{2}$. In order to simplify our presentation, we study the linearisation in the coordinates given by e_{11} and $e_{11}^{\perp}$ (see Lemma 3.3 below for a justification).

The linearisation of the wells is given by

$$E_j = \frac{d}{d\alpha}\left[e(H_j(\alpha))\right]|_{\alpha=\frac{1}{2}},$$

where $e(M) := \frac{1}{2}(M + M^T)$ denotes the symmetrised part of a matrix $M \in \mathbb{R}^{2\times 2}$ and $H_j(\alpha) := \nabla u|_{T_j}$ is the restriction of the piecewise constant function ∇u from Theorem 1 (ii) (which in particular depends on α). In particular,

$$E_1 = \begin{pmatrix} 1 & -\frac{\cos(\phi_n/2)}{\sin(\phi_n/2)} \\ -\frac{\cos(\phi_n/2)}{\sin(\phi_n/2)} & -1 \end{pmatrix}, \tag{58}$$

and

$$E_2 = \begin{pmatrix} 1 & \frac{\cos(\phi_n/2)}{\sin(\phi_n/2)} \\ \frac{\cos(\phi_n/2)}{\sin(\phi_n/2)} & -1 \end{pmatrix}.$$

In order to justify our linearisation (in the α dependent choice of coordinates), we note the following:

Lemma 3.3. *For each $\alpha \in (0,1)$ let $e_{11}, e_{11}^{\perp}$ denote the (α dependent) coordinates from Section 2.1.1. Then, we have*

$$\begin{aligned}&\frac{d}{d\alpha}\left[(e_{11}\ e_{11}^{\perp})e(H_j(\alpha))(e_{11}\ e_{11}^{\perp})^T\right]\big|_{\alpha=\frac{1}{2}}\\&= (e_{11}\ e_{11}^{\perp})\big|_{\alpha=\frac{1}{2}}\left(\frac{d}{d\alpha}e(H_j(\alpha))\big|_{\alpha=\frac{1}{2}}\right)(e_{11}\ e_{11}^{\perp})^T\big|_{\alpha=\frac{1}{2}}.\end{aligned}$$

As a consequence and as expected, it does not matter in which coordinates we consider the geometric linearisation of the problem at hand. Hence, in the sequel, without further comment, we will always consider the linearisation in the coordinates $(e_{11}\ e_{11}^{\perp})\big|_{\alpha=\frac{1}{2}}$.

Proof. We show that for a general rotation Q which depends differentiably on the parameter α, we have

$$\frac{d}{d\alpha}\left[Qe(H_j(\alpha))Q^T\right]\big|_{\alpha=\frac{1}{2}} = Q\big|_{\alpha=\frac{1}{2}}\left(\frac{d}{d\alpha}e(H_j(\alpha))\big|_{\alpha=\frac{1}{2}}\right)Q^T\big|_{\alpha=\frac{1}{2}}.$$

Indeed, this is a direct consequence of the product rule. Denoting derivatives with respect to α by a dash, we obtain

$$\begin{aligned}\frac{d}{d\alpha}\left[Qe(H_j(\alpha))Q^T\right]\big|_{\alpha=\frac{1}{2}} &= Q'\big|_{\alpha=\frac{1}{2}}e(H_j(\alpha))\big|_{\alpha=\frac{1}{2}}Q^T\big|_{\alpha=\frac{1}{2}}\\&\quad + Q\big|_{\alpha=\frac{1}{2}}[e(H_j(\alpha))]'\big|_{\alpha=\frac{1}{2}}Q^T\big|_{\alpha=\frac{1}{2}}\\&\quad + Q\big|_{\alpha=\frac{1}{2}}e(H_j(\alpha))\big|_{\alpha=\frac{1}{2}}(Q^T)'\big|_{\alpha=\frac{1}{2}}.\end{aligned}\tag{59}$$

Now, using that

$$Q'\big|_{\alpha=\frac{1}{2}} = c\begin{pmatrix}0 & 1\\ -1 & 0\end{pmatrix}Q\big|_{\alpha=\frac{1}{2}},$$

and the fact that $[e(H_j(\alpha))]'\big|_{\alpha=\frac{1}{2}} \in \frac{1}{\cos(\frac{\pi}{n})}(O(2)\setminus SO(2))\cap\mathbb{R}^{2\times 2}_{sym}$, implies by the commutation relations for rotations and reflections that the first and second contributions in (59) cancel. Thus, we obtain the desired result. □

As a direct consequence of the non-linear constructions from the previous Sections 2.1.3, we obtain the following geometrically linearised Conti constructions:

Proposition 3.4. *Let $u_\alpha : \mathbb{R}^2 \to \mathbb{R}^2$ be a non-linear deformation associated with a non-linear Conti construction with $\alpha \in (0,1)$. Then the function $v_0 := \frac{d}{d\alpha}u_\alpha\big|_{\alpha=\frac{1}{2}} : \mathbb{R}^2 \to \mathbb{R}^2$ is a displacement vector field for a geometrically linear Conti construction, i.e. it is a piecewise affine, continuous vector field, which has constant gradient on the triangles $T_1, \dots, T_{2n}$. The symmetrised gradients involved in the linearised construction are given by the matrices $E_1, \dots, E_{2n}$ corresponding to the linearisations and symmetrisations of $H_1(a(\alpha)), \dots, H_{2n}(a(\alpha))$. In the exterior of the polygon Ω_n^E and in the polygon Ω_n^I, the displacement gradient is a skew matrix.*

Remark 3.5. *As a consequence of the linearisation results and the remarks on the symmetry of the geometrically non-linear construction (see Corollary 2.4 and the remarks following it), the results of Proposition 3.4 also imply parts of the claims of Theorem 2. The claims on the number of wells will be proved in Section 3.3.1. Further, in Section 3.3.2 we provide a second proof of Theorem 2 which directly works with the geometrically linearised set-up and does not rely on exploiting the previous arguments on the non-linear construction.*

Proof. We first note that, by the explicit expressions from Section 2.1 for any $\alpha > 0$ the deformation u_α depends differentiably on the parameter α. Thus, in order to prove that v_0 is a displacement for the geometrically linear Conti construction, it suffices to show that v_0 is continuous along the sides of the triangles $T_1, \dots, T_{2n}$. Let $\ell_\alpha : \mathbb{R}^2 \to \mathbb{R}^2$ be a line segment with normal $\nu_\alpha \in \mathbb{R}^2$ describing one of the edges of the triangles $T_1, \dots, T_{2n}$. Let $x \in \ell_\alpha$ and denote by $\ell_\alpha^+(x)$ denote the limit of points $y \in \mathbb{R}^2$ with $y \cdot \nu_\alpha \geq 0$ and $y \to x$. Define $\ell_\alpha^-(x)$ similarly. Then, by continuity of u_α for all $\alpha > 0$ we in particular have that for all $x \in \ell_\alpha$

$$u_\alpha(\ell_\alpha^+(x)) - u_\alpha(\ell_\alpha^-(x)) = 0.$$

As a consequence,

$$\frac{d}{d\alpha}\left[u_\alpha(\ell_\alpha^+(x)) - u_\alpha(\ell_\alpha^-(x))\right]\Big|_{\alpha=\frac{1}{2}} = 0.$$

By the product rule this however turns into

$$0 = \left[v_0(\ell_1^+(x)) - v_0(\ell_1^-(x))\right] + \left[u_1(x)(\ell'_{1,+}(x)) - u_1(x)(\ell'_{1,-}(x))\right], \tag{60}$$

where $\ell'_{1,\pm}(x) := \left[\frac{d}{\alpha}\ell_\alpha^\pm(x)\right]\big|_{\alpha=\frac{1}{2}}$. By the C^1 continuity of $\ell_\alpha(x)$ we however have $\ell'_{1,+}(x) = \ell'_{1,-}(x)$. Hence, the continuity of u_1 implies that (60) turns into

$$0 = \left[v_0(\ell_1^+(x)) - v_0(\ell_1^-(x))\right].$$

This is the claimed continuity of v_0 along the edges of the triangles. □

Remark 3.6. *As a direct consequence of the derivation of the linear displacement u_α from the non-linear constructions from Section 2.1, we also obtain the symmetrised rank-one directions from the rank-one directions of the non-linear problem: Let $H_1 - H_2 = \frac{\cos(\phi_n/2)}{\sin(\phi_n/2)} e_1 \otimes e_2$. Then the matrices E_1, E_2 obtained as above, satisfy*

$$E_1 - E_2 = \frac{\cos(\phi_n/2)}{\sin(\phi_n/2)} e(e_1 \otimes e_2).$$

3.3.1. *Remarks on the number of wells.* We discuss the number of wells that are involved in the geometrically linearised Conti-type constructions from Proposition 3.4 in more detail. As discussed in Remark 2.5, it will turn out that in contrast to the geometrically non-linear setting, in the geometrically linearised setting only n wells are needed for a single onion layer construction, *independently* of whether n is odd or even (we recall that in the geometrically non-linear setting $2n$ wells were needed if n was odd). This follows from Corollary 3.4, the values of the strains which are used there and the interaction of the linearisation with the symmetry group $\mathcal{P}_n$. Although this also directly follows by combining the results from Section 3.3.2 with the linearisation procedure, we give an independent proof which highlights the structure of the linear wells. In the next section, we will then study the iterability of the single onion ring layer constructions in the geometrically linearised setting.

Lemma 3.7. *Let $n \in \mathbb{N}$, $n \geq 3$ be odd and let*

$$K = \{RE_1R^T : \ R \in \hat{\mathcal{P}}_n\}, \tag{61}$$

where $\hat{\mathcal{P}}_n := \hat{\mathcal{R}}_1^n \cup \hat{\mathcal{R}}_2^n$ is defined as in (47). Then the single layer Conti construction obtained in Proposition 3.4 is such that exactly n different strains are used. More generally, the set of linearised energy wells K consists of exactly n different wells, i.e. $\#K = n$.

Remark 3.8. *Here and in the sequel, we work with the symmetry group $\hat{\mathcal{P}}_n$ instead of the group $\mathcal{P}_n$ since we are considering the problem in the $e_{11}, e_{11}^\perp$ coordinates.*

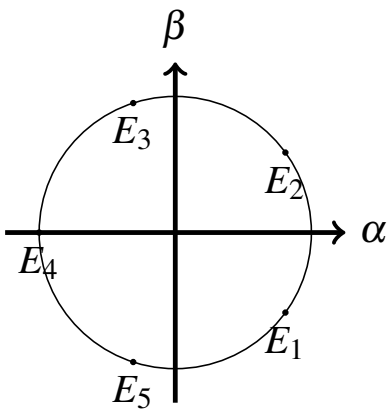

FIGURE 7. The geometrically linearised n-well problem for $n = 5$. As exploited in the proof of Lemma 3.7, the set K can be parametrised through a vector (α, β), i.e. each element of K is of the form $\begin{pmatrix} \alpha & \beta \\ \beta & -\alpha \end{pmatrix}$ with $\alpha^2 + \beta^2 = const.$ Hence, by the identities from the properties (i), (ii) in the proof of Lemma 3.7, it is possible to visualise the set of wells as a regular n-gon as illustrated in this figure.

Proof. We first prove that $\#K \leq n$, the fact that $\#K = n$ will be a consequence of the argument for this.

The symmetry group $\hat{\mathcal{P}}_n$ acts on K by conjugation. In particular, K is obtained as the orbit of E_1 under conjugation with elements of $\hat{\mathcal{P}}_n$. As $\hat{\mathcal{P}}_n \subset O(2)$, we more generally consider the conjugation class of the matrix $\begin{pmatrix} 1 & d \\ d & -1 \end{pmatrix}$ for $d \in \mathbb{R}$ (which is of the same structure as E_1) under $O(2)$.

Since

$$\begin{aligned} O(2) &= SO(2) \cup \begin{pmatrix} -1 & 0 \\ 0 & 1 \end{pmatrix} SO(2) \\ &= \left\{ \begin{pmatrix} a & b \\ -b & a \end{pmatrix} \cup \begin{pmatrix} a & -b \\ -b & -a \end{pmatrix} : \ a, b \in \mathbb{R} \text{ such that } a^2 + b^2 = 1 \right\}, \end{aligned}$$

on the one hand, we compute

$$\begin{pmatrix} a & b \\ -b & a \end{pmatrix} \begin{pmatrix} 1 & d \\ d & -1 \end{pmatrix} \begin{pmatrix} a & -b \\ b & a \end{pmatrix} = \begin{pmatrix} a^2 + 2abd - b^2 & -2ab + a^2 d - b^2 d \\ -2ab + a^2 d - b^2 d & b^2 - 2abd - a^2 \end{pmatrix}. \tag{62}$$

On the other hand, we also have

$$\begin{pmatrix} a & b \\ b & -a \end{pmatrix} \begin{pmatrix} 1 & d \\ d & -1 \end{pmatrix} \begin{pmatrix} a & b \\ b & -a \end{pmatrix} = \begin{pmatrix} a^2 + 2abd - b^2 & 2ab - a^2 d + b^2 d \\ 2ab - a^2 d + b^2 d & b^2 - 2abd - a^2 \end{pmatrix}. \tag{63}$$

Comparing the matrix in (62) with the one in (63), we note that the diagonal entries agree, while the off-diagonal ones deviate by a sign. Letting $\hat{\mathcal{R}}_1^n := \hat{\mathcal{P}}_n \cap SO(2)$ and $\hat{\mathcal{R}}_2^n = \hat{\mathcal{P}}_n \setminus \hat{\mathcal{R}}_1^n$, we study the orbit of E_1 under the action of $\hat{\mathcal{R}}_1^n$. It has the following properties:

(i) The orbit of E_1 under $\hat{\mathcal{R}}_1^n$ forms a regular n-gon in trace-free strain space parametrised as matrices of the form

$$\begin{pmatrix} \alpha & \beta \\ \beta & -\alpha \end{pmatrix}, \ \alpha, \beta \in \mathbb{R},$$

see Figure 7.

(ii) For $c = \frac{1}{\cos(\frac{\pi}{n})}$ the matrix $c \begin{pmatrix} -1 & 0 \\ 0 & 1 \end{pmatrix}$ is an element of this n-gon.

Both properties (i) and (ii) follow from trigonometric identities: For (i) we note that as $\begin{pmatrix} \alpha & \beta \\ \beta & -\alpha \end{pmatrix} \in (\alpha^2 + \beta^2)(O(2) \setminus SO(2))$ by the commutation relations for rotations and reflections, we have

$$\begin{aligned} &\begin{pmatrix} \cos(\varphi) & -\sin(\varphi) \\ \sin(\varphi) & \cos(\varphi) \end{pmatrix} \begin{pmatrix} \alpha & \beta \\ \beta & -\alpha \end{pmatrix} \begin{pmatrix} \cos(\varphi) & \sin(\varphi) \\ -\sin(\varphi) & \cos(\varphi) \end{pmatrix} \\ &= \begin{pmatrix} \cos(2\varphi) & -\sin(2\varphi) \\ \sin(2\varphi) & \cos(2\varphi) \end{pmatrix} \begin{pmatrix} \alpha & \beta \\ \beta & -\alpha \end{pmatrix}. \end{aligned} \tag{64}$$

Hence, conjugating a matrix $\begin{pmatrix} \alpha & \beta \\ \beta & -\alpha \end{pmatrix}$ by a rotation with angle φ just rotates the matrix $\begin{pmatrix} \alpha & \beta \\ \beta & -\alpha \end{pmatrix}$ by the angle 2φ. As a consequence, we note that as n is odd, the orbit of E_1 under $\mathcal{R}_1^n$ is exactly given by a regular n-gon (as starting from E_1 we first reach all elements of the orbit which are at the even lattice sites of the n-gon with respect to the starting point E_1 and then after continuing to rotate, we also obtain the odd ones).

In order to deduce the second property (ii), we first study under which conditions the off-diagonal entry in (62) vanishes. In order to simplify notation, we set $a = \cos(\varphi)$, $b = \sin(\varphi)$ with $\varphi = \frac{2\pi j}{n}$, $j \in \mathbb{Z}$, and $d = \cot(\phi_n/2)$, and note that then

$$2ab - a^2 d + b^2 d = \frac{1}{\cos\left(\frac{\pi}{n}\right)} \cos\left(\frac{\pi - 4j\pi}{n}\right). \tag{65}$$

In order to prove the claim in (ii), we search for values of j such that this expression vanishes. Hence, we seek an integer j such that $1 - 4j \in n\mathbb{Z}$. This is solved by

$$j = \begin{cases} \frac{n+1}{4}, & \text{if } n \equiv 3 \pmod 4, \\ \frac{3n+1}{4}, & \text{if } n \equiv 1 \pmod 4. \end{cases}$$

The claim (i) then follows as the expression $a^2 - 2abd - b^2$ in (62) turns into $\frac{\cos(\frac{\pi - 4j\pi}{n})}{\cos(\frac{\pi}{n})} = \frac{-1}{\cos(\frac{\pi}{n})}$.

With the properties (i), (ii) at hand, by the symmetry of the n-gon, we infer that the orbit of E_1 under the action of the group $\hat{\mathcal{R}}_1^n$ contains the matrix $\begin{pmatrix} g & -f \\ -f & -g \end{pmatrix}$, iff it contains the matrix $\begin{pmatrix} g & f \\ f & -g \end{pmatrix}$. In particular, this implies that if a matrix of the form (62) is contained in the orbit of E_1 under $\hat{\mathcal{R}}_1^n$, also the corresponding matrix in (63) is already contained in the orbit of E_1 under $\hat{\mathcal{R}}_1^n$. As a consequence, the orbit of E_1 under $\hat{\mathcal{R}}_2^n$ does not contain new information and $\#K \leq n$.

The observation that $\#K \geq n$ is a direct consequence of property (i) from above, which thus yields $\#K = n$ and which concludes the argument. □

3.3.2. *Proof of Theorem 2.* Although Theorem 2 is a direct consequence of the corresponding properties of the geometrically non-linear problem (see Section 3.3.2) and the linearisation results proved in the previous subsection, we provide a second,

self-contained proof here, as the geometrically linear setting allows for significant computational simplifications compared to the geometrically non-linear situation.

Proof of Theorem 2. We recall our convention on the notation for rotations from (20). The fact that

$$e(\nabla \tilde{v}_n) \in \{E_1, \dots, E_n\} := \left\{Q_j E_1 Q_j^T : \ j \in \{0, \dots, n-1\}\right\}$$

follows from the observation that the symmetrised gradients are obtained by linearisation of the iterated non-linear construction (here Q_α denotes the rotation from Section 3.3.2). Indeed, by the same considerations as in Lemma 3.3 we infer that

$$\begin{aligned}
&\frac{d}{d\alpha}\left(Q_\alpha e(\nabla v_{\alpha,n}) Q_\alpha^T\right)|_{\alpha=\frac{1}{2}} \\
&= (Q_\alpha' e(\nabla v_{\alpha,n}) Q_\alpha^T)|_{\alpha=\frac{1}{2}} + (Q_\alpha e(\nabla v_{\alpha,n})' Q_\alpha^T)|_{\alpha=\frac{1}{2}} + (Q_\alpha e(\nabla v_{\alpha,n})(Q_\alpha')^T)|_{\alpha=\frac{1}{2}} \\
&= (Q_\alpha')|_{\alpha=\frac{1}{2}} e(\nabla v_{\frac{1}{2},n}) R_{\frac{1}{2}}^T + R_{\frac{1}{2}} e(\nabla \tilde{v}_{\frac{1}{2},n}) R_{\frac{1}{2}}^T + R_{\frac{1}{2}} e(\nabla v_{\frac{1}{2},n})(Q_\alpha')^T|_{\alpha=\frac{1}{2}} \\
&= R_{\frac{1}{2}} e(\nabla \tilde{v}_{\frac{1}{2},n}) R_{\frac{1}{2}}^T.
\end{aligned}$$

Here the dash denotes differentiation with respect to α; moreover, we used that

$$e(\nabla v_{\frac{1}{2},n}) = Id, \ Q_\alpha' = \begin{pmatrix} 0 & 1 \\ -1 & 0 \end{pmatrix} Q_\alpha.$$

As $R_{\frac{1}{2}} \in \hat{\mathcal{P}}_n$, this proves the claim on the inclusion.

In order to prove (i), by symmetry it suffices to prove the claim for $j = 1$ and $j = 2$. Since $Q_{\frac{n}{2}} = Q(\pi)$, the result is straightforward for $j = 2$. We thus focus on the case $j = 1$ for which we need to prove that

$$Q_{\frac{n-1}{2}} P_0 E_1 P_0 Q_{\frac{n-1}{2}}^T = E_1.$$

This however follows from the following observations:

- By the explicit form of E_1, we have $E_1 \in \frac{1}{\sin(\frac{\pi}{n})} SO(2)$, whence by the commutation relations for reflections and rotations,
$$P_0 E_1 P_0 = E_2,$$
(the action of P_0 just flips the sign in the off-diagonal component).
- By a similar reasoning (see 64) we then also obtain that
$$Q_{\frac{n-1}{2}} E_2 Q_{\frac{n-1}{2}}^T = Q_{n-1} E_2.$$
- By the structure of the set of E_j, we however have $Q_{n-1} E_2 = E_1$ (more generally, we have $E_j = Q_j E_1$ for all odd j).

As a consequence, by combining the previous observations

$$Q_{\frac{n-1}{2}} P_0 E_1 P_0 Q_{\frac{n-1}{2}}^T = Q_{\frac{n-1}{2}} E_2 Q_{\frac{n-1}{2}}^T = Q_{n-1} E_2 = E_1,$$

which yields the desired result.

Finally, we provide the argument for (ii): Again we consider only the case $j = 1$ and $j = 2$. Considering first the case $j = 1$, we note that

$$R_{\frac{1}{2}} E_2 R_{-\frac{1}{2}} = R_{\frac{1}{2}} P_0 E_1 P_0 R_{-\frac{1}{2}} = Q_{\frac{1}{2}} P_0 E_1 P_0 Q_{\frac{1}{2}}^T.$$

It hence suffices to prove that

$$Q_1 E_1 Q_1^T = Q_{\frac{1}{2}} P_0 E_1 P_0 Q_{\frac{1}{2}}^T.$$

This however is equivalent to

$$Q_1 E_1 Q_1^T = P_0 E_1 P_0 = E_2.$$

Since by (64), we have

$$Q_{\frac{1}{2}} E_1 Q_{\frac{1}{2}}^T = Q_1 E_1 = E_2,$$

the claim follows for $j = 1$. The argument for $j = 2$ is analogous. □

4. The Limit $N \to \infty$

As explained in the introduction, the specific solutions to the differential inclusion which we consider in this article allow us to treat Conti-type constructions for elastic crystals and nematic liquid crystal elastomers within a unified framework.

Thus, equipped with the finite n construction from the Sections 2 and 3, in this section, we discuss the passage to the limit $n \to \infty$ both in the geometrically non-linear and the geometrically linearised theories. Physically, the limit $n \to \infty$ corresponds to the nematic liquid crystal elastomer limit. We emphasise that, however, also the finite n constructions might be of interest in the nematic elastomer context as they could serve as bench marks for numerical simulations (see the discussion below). Moreover, as all our finite n constructions also represent a possible nucleation mechanisms for the nematic elastomer case, the polygonal domain geometry might serve as a selection mechanism choosing a finite number out of the infinitely many possible energy wells.

4.1. **Results on the limit $n \to \infty$ in the geometrically non-linear setting.** We begin by discussing the limit of the construction from Theorem 1 (ii) and will construct exactly stress-free (two-dimensional) solutions to the nematic elastomer problem (see Corollary 4.4). In the sequel, we will refer to the notation from Theorem 1 (ii) and also from Section 2.1.2. Further we recall our convention on the notation for rotations from (20) and that our finite n constructions depended on only two parameters – the $n-$gon parameter n and the rotation angle α. Next we observe that, due to (15), for a single layer construction the ratio of the inner and outer radii converges to one another as $n \to \infty$:

$$\frac{r_I}{r_E} = 1 - \frac{2\pi\sqrt{\alpha(1-\alpha)}}{n} + O(n^{-2}) \text{ as } n \to \infty.$$

Hence, in order to observe a non-trivial limiting configuration as $n \to \infty$, in the sequel, we iterate more and more layers of our construction for finite n (as discussed in Section 3.3.2).

Let us explain this in more detail. Without loss of generality, below we consider $v_n := R_E u_n$, where as in the proof of Theorem 1 (ii), R_E is such that $\nabla v_n|_{T_1} = H$ and where H is as in (17) (cf. the proof of Theorem 1 (ii) in Section 3.1.1). As in Section 2.2, we now fix $\alpha > 0$, set for a matter of simplicity $r_E = 1$, take r_I satisfying (15) and consider the iterated layer solution

$$v_n(x) = \sum_{k=0}^{N_n} r_I^k R_E R_*^k Q_\alpha^k u(r_I^{-k} Q_{-\alpha}^k x)\chi_{\Sigma_k} + R_E x \chi_{\mathbb{R}^2 \setminus \Sigma_0^{co}} + R_E R_*^{N_n+1} x \chi_{\overline{\Sigma}_{N_n+1}^{co}},$$

where χ_B is the indicator function on the set B, R_* is as in (iv), Q_α is a rotation of angle $\frac{2\pi}{n}\alpha$ and the sets Σ_i are defined by

$$\Sigma_i := \{x \in \mathbb{R}^2 : |x| \in r_I^i Q_\alpha^i \Omega_n\}.$$

Again, we choose the positive integer N_n such that $N_n := \inf\{N \in \mathbb{N} : r_I^N \leq \frac{1}{2}\}$.

Below we denote by B_r the open ball centred at zero and of radius r. With this notation in hand, we pass to the limit $n \to \infty$, thus, physically passing to the liquid crystal elastomer regime (see the discussion below).

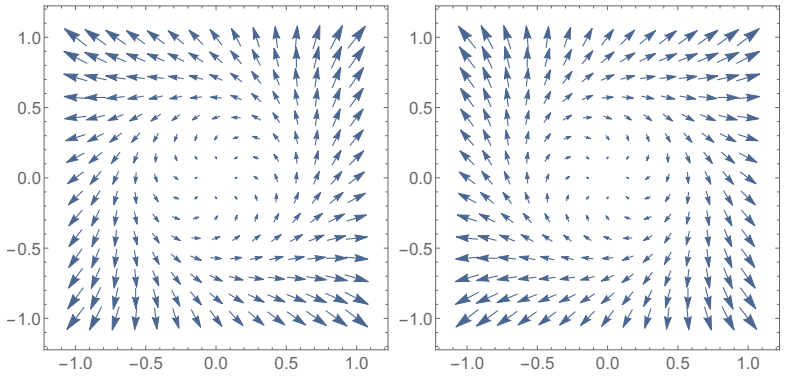

FIGURE 8. Vector plot of $v(x)$ for $\alpha = 0.2$ (left) and $\alpha = 0.8$ (right).

Proposition 4.1. *Let $\alpha \in (0,1)$, then there exists $v \in W^{1,\infty}_{loc}(\mathbb{R}^2;\mathbb{R}^2)$ such that $v_n \to v$ in the $W^{1,p}_{loc}(\mathbb{R}^2;\mathbb{R}^2)-$norm for each $p \geq 1$, and $\nabla v = Q(\beta_0)$ on $\mathbb{R}^2 \setminus B_1$, $\nabla v = Q(\beta_0)Q(\rho_0 \log \frac{1}{2})$ on $B_{1/2}$ and*

$$\nabla v = Q(\rho_0 \log r)Q(\omega)\big(a\bar{e}_{11} \otimes \bar{e}_{11} + a^{-1}\bar{e}_{11}^{\perp} \otimes \bar{e}_{11}^{\perp}\big)Q^T(\omega), \qquad \text{in } B_1 \setminus B_{\frac{1}{2}},$$

where $Q(s)$ denotes the rotation of angle $s \in \mathbb{R}$, $\rho_0 = \frac{2\alpha-1}{\sqrt{\alpha(1-\alpha)}}$, $\beta_0 = \sin^{-1}(1-2\alpha)$, $r = |x|$ and $\omega = \arctan\left(\frac{x\cdot e_2}{x\cdot e_1}\right)$. Furthermore, $a = \sqrt{\frac{1-\alpha}{\alpha}}$ and $\bar{e}_{11} = (\sqrt{1-\alpha}, -\sqrt{\alpha})$.

Remark 4.2. *If we seek to emphasise the dependence of the limiting deformation v on a, we also use the notation v_a.*

With the results of Proposition 4.1 in hand, we can also compute the associated deformation:

Corollary 4.3. *Let $\alpha \in (0,1)$. Then, we have*

$$v_n(x) \to v_a(x) := rQ(\omega + \rho_0 \log(r)) \begin{pmatrix} 2\sqrt{\alpha(1-\alpha)} \\ 1-2\alpha \end{pmatrix},$$

uniformly in $B_1 \setminus B_{\frac{1}{2}}$.

Physically these solutions are of interest, as for each fixed $\alpha \in (0,1)$ our constructions also yield exactly stress-free solutions to the full (two-dimensional) nematic elastomer inclusion problem:

Corollary 4.4. *Let $K_n(a) := \bigcup_{P \in \mathcal{P}_n} SO(2)PH(a)P^T$, where $H(a)$ is as in (17). Then, as $n \to \infty$, it converges in a pointwise sense to the set*

$$\begin{aligned} K_\infty(a) &:= \bigcup_{P \in O(2)} SO(2)PH_\infty(a)P^T \\ &= \{F \in \mathbb{R}^{2\times 2} : \ \det(F) = 1, \ \lambda(F) = a, \ \mu(F) = a^{-1}\}, \end{aligned} \tag{66}$$

where $H_\infty(a) := a\bar{e}_{11} \otimes \bar{e}_{11} + \frac{1}{a}\bar{e}_{11}^{\perp} \otimes \bar{e}_{11}^{\perp}$, $\bar{e}_{11}$ is as in Proposition 4.1 and where $\lambda(F), \mu(F)$ denote the singular values of the matrix F. In particular, the deformation v from Proposition 4.1 is a solution to the differential inclusion

$$\nabla v \in K_\infty(a) \text{ in } B_1.$$

Seeking to view the constructions for finite n and the limit $n \to \infty$ both in the contexts of solid and nematic liquid crystal elastomers, we explain a precise sense in which (66) can be understood as the energy wells for a planar nematic liquid crystal elastomer differential inclusion. This, in particular, allows us to view the

deformation v from Proposition 4.1 and Corollary 2.4 as a microstructure arising in the modelling of certain planar deformations in nematic liquid crystal elastomers.

To this end, we begin by investigating planar solutions to the geometrically non-linear, nematic elastomer differential inclusion (5). More precisely, we consider $u : B_1(0) \times [0,1] \to \mathbb{R}^3$ which is of the form

$$u(x_1, x_2, x_3) = (\tilde{u}(x_1, x_2), 0) + \left[\begin{pmatrix} 0 & 0 \\ 0 & r^{-\frac{1}{6}} \end{pmatrix} x \right]^T.$$

Here $r^{-\frac{1}{3}}$ is one of the constants from (5) and we assume that $\tilde{u}(x_1, x_2) = M'(x_1, x_2)$ on $\partial\Omega$ for some $M' \in \mathbb{R}^{2\times 2}$. Seeking an exactly stress-free deformation within the framework of the BWT model (5), the two eigenvalues of $\nabla' \tilde{u}$ are therefore determined by the differential inclusion $\nabla u \in \tilde{K}_\infty$ with $\tilde{K}_\infty$ as in (9). Here the notation $\nabla' \tilde{u}$ refers to the gradient of $\tilde{u}$ in the x_1, x_2 directions. Without loss of generality assuming that $r > 1$ and with slight abuse of notation, the singular values are thus given by $\lambda_1 = r^{-\frac{1}{6}}$ and $\lambda_2 = r^{\frac{1}{3}}$. In other words, in order to solve the differential inclusion $\nabla u \in \tilde{K}_\infty(r)$, it is necessary and sufficient that

$$\nabla' \tilde{u} \in K_{2D}(r), \tag{67}$$

where

$$K_{2D}(r) := \{F \in \mathbb{R}^{2\times 2} : \ \lambda_1(F) = r^{-\frac{1}{6}}, \ \lambda_2(F) = r^{\frac{1}{3}}, \ \det(F) = r^{\frac{1}{6}}\}. \tag{68}$$

We note that the set in (68) coincides with the set from Corollary 4.4 up to a rescaling which modifies the determinant, i.e., $K_{2D}(r) = r^{\frac{1}{12}} K_\infty(r^{\frac{1}{4}})$.

By the theory of relaxation (see for instance [DM12, Dac07]), interesting microstructures arise if

$$M' \in \operatorname{int} K_{2D}^{qc}(r) := \{F \in \mathbb{R}^{2\times 2} : \ r^{-\frac{1}{6}} < \lambda_1(\nabla \tilde{u}) \leq \lambda_2(\nabla \tilde{u}) < r^{\frac{1}{3}}, \ \det(F) = r^{\frac{1}{6}}\}.$$

In particular, we obtain that for $a = r^{\frac{1}{4}}$ the deformation $r^{\frac{1}{12}} v$ from Proposition 4.1 and Corollary 2.4 is a solution to the differential inclusion (67) with a non-trivial microstructure.

Concluding our discussion on the geometrically non-linear theory, we present examples of director fields minimising the energy density of nematic elastomers in Figures 9-10. Here the planar deformation gradient $\nabla u(x)$ is obtained as an exact solution in the sense that we have $\nabla u \in K_{2D}(r)$, where it is imagined to be the 2×2 planar deformation associated with a full 3×3 volume-preserving deformation. Consequently, the nematic elastomer is in planar expansion in all the deformed configurations for $a > 1$. The planar director field is taken in the form $\hat{n}(x) = (\cos\theta, \sin\theta, 0)$ and it corresponds to the eigenvector associated with the largest eigenvalue of $\nabla u \nabla u^T$, in agreement with (8). More exact constructions are displayed in Figure 10 for large nematic anisotropies at finite n. These correspond to solutions

$$\nabla u \in K_n(a),$$

which however can always also be interpreted as a nematic elastomer inclusion problem as

$$K_n(a) \subset r_n^{\frac{1}{12}} K_{2D}(r_n),$$

where $r_n > 0$ is a function of n, a. Although an anisotropy parameter of the order $r_n = O(10^2)$ is non-physical, we report these solutions as they represent nice examples of the theory developed in this article showing large deformations and director rotation.

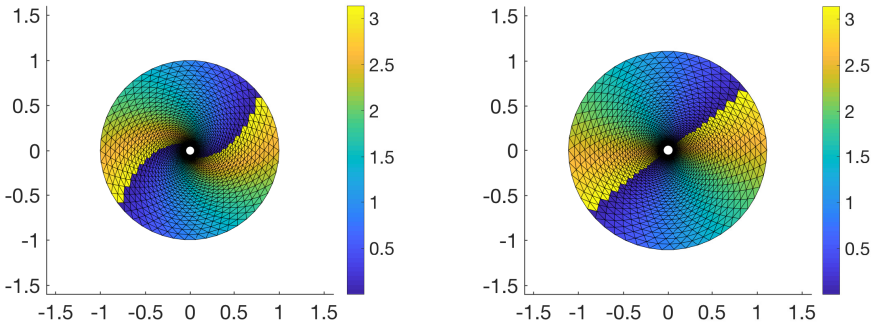

FIGURE 9. Example of planar director fields that minimise pointwise the energy density for nematic elastomers. Directors are parametrised as $\hat{n} = (\cos\theta, \sin\theta, 0)$ and the value of θ is represented by means of a colourmap. Recall due to the head-tail symmetry the orientation of the molecules is fully described by $\hat{n} \otimes \hat{n}$ and therefore there is no discontinuity in the field of orientation of the molecules in passing from $\theta = 0$ to $\theta = \pi$. Here $\alpha = 0.35$, $n = 50$ for which we have $r_{50} \approx 3.5$. The director field is displayed in the reference configuration (left) and in the deformed configuration (right). Observe the planar expansion as $r_n > 1$.

Observe that the solutions obtained for finite n for the *discrete* NLCEs model still survive as exact solutions of nematic elastomer configurations since $\mathcal{P}_n \subset O(2)$. A possible application of the discrete model of NLCEs thus obtained for finite n is for benchmarking of large numerical simulations. Here the advantage is that the discrete modelling approach involves only a finite subsets of energy wells and has the potential to provide a faster and more stable energy minimisation with respect to the full isotropic NLCEs model.

4.2. **Proofs on the limit $n \to \infty$ in the geometrically nonlinear theory.** In this section we present the proofs on the passage to the limit $n \to \infty$.

Proof of Proposition 4.1. We have that $v_n(x) = R_E x$ in $\mathbb{R}^2 \setminus B_1$ for every n. As $n \to \infty$, the rotation matrix $R_E \to Q(\sin^{-1}(1-2\alpha))$, a rotation of angle $\sin^{-1}(1-2\alpha)$. Indeed, R_E is such that $R_E \overline{E_1E_2} = P_0HP_0\overline{E_1E_2}$, and hence the angle β_0 of R_E is given by

$$\beta_0 = \sin^{-1} \frac{\overline{E_1E_2} \times P_0HP_0\overline{E_1E_2}}{|\overline{E_1E_2}||P_0HP_0\overline{E_1E_2}|}.$$

We recall that

$$\overline{E_1E_2} = l_2 e_{11} - l_1 e_{12},$$
$$P_0HP_0\overline{E_1E_2} = a l_2 e_{11} - \frac{l_1}{a} e_{12}.$$

and that by (40)–(41)

$$|P_0HP_0\overline{E_1E_2}|^2 = |\overline{E_1E_2}| = l_2^2(1 + a^2 + 2a\sin\frac{\pi}{n}).$$

Using (34) we deduce that

$$\beta_0 = \sin^{-1} \frac{(a^2-1)\cos\frac{\pi}{n}}{1 + a^2 + 2a\sin\frac{\pi}{n}} \to \sin^{-1}(1-2\alpha)$$

as $n \to \infty$.

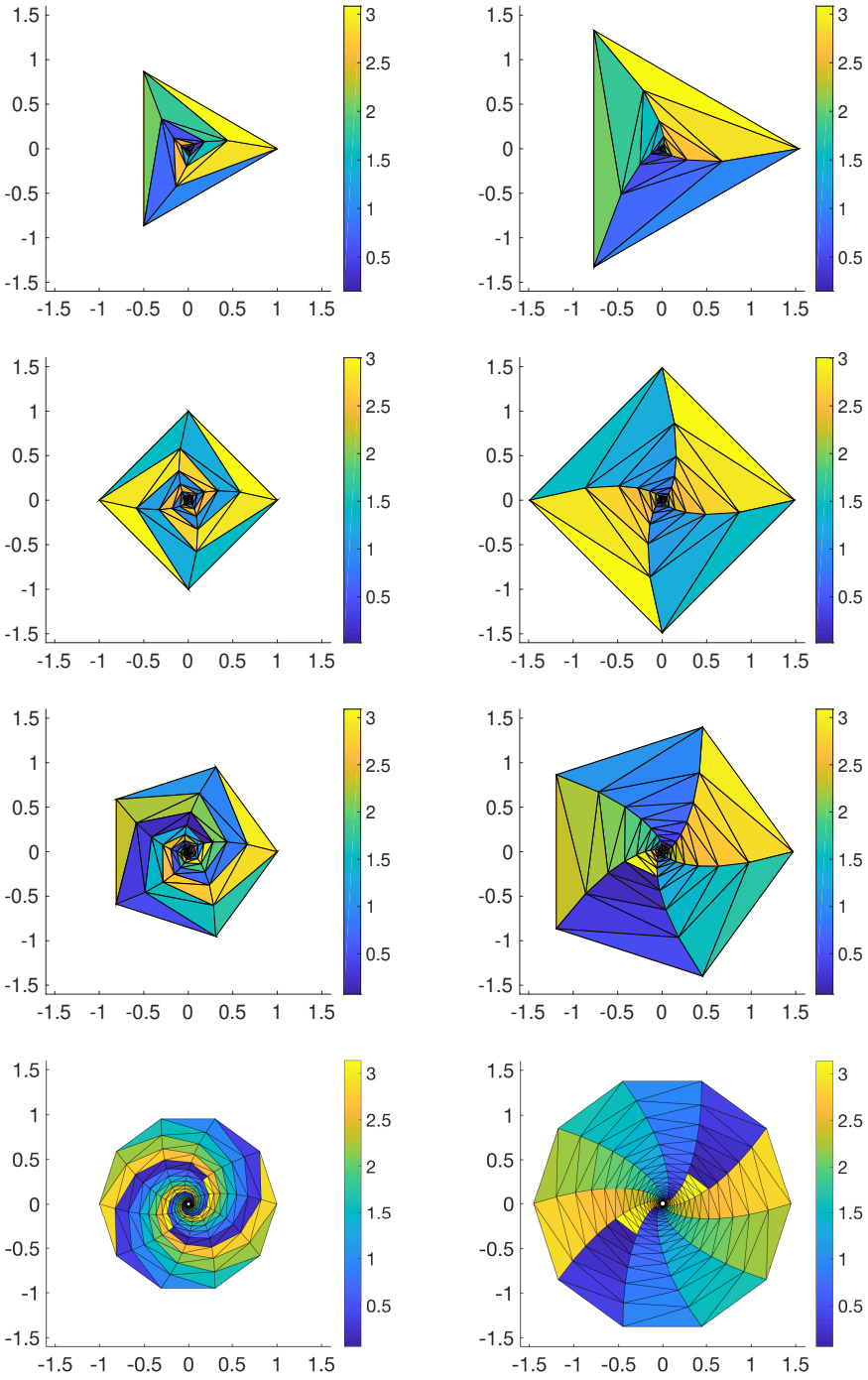

FIGURE 10. More examples of planar director fields obtained for large values of the nematic anisotropy parameter r_n. Here $\alpha = 0.1$. From top to bottom, $n = 3$ ($r_3 \approx 171$), $n = 4$ ($r_4 \approx 118$), $n = 5$ ($r_5 \approx 102$) and $n = 10$ ($r_{10} \approx 85$) respectively. The director field is displayed in the reference configuration (left) and in the deformed configuration (right). Observe a large planar expansion as $r_n \gg 1$.

Therefore, we focus on the deformation in B_1 and notice that since v_n is a bounded sequence in $W^{1,\infty}(B_1;\mathbb{R}^2)$, there exists $\tilde{v} \in W^{1,\infty}(B_1;\mathbb{R}^2)$ with $\tilde{v}|_{\partial B_1} = R_E x$, and a non relabelled subsequence such that $v_n \to \tilde{v}$ weakly$-*$ in $W^{1,\infty}(B_1;\mathbb{R}^2)$, uniformly in $C(B_1;\mathbb{R}^2)$. We now claim that $\nabla v_n \to \nabla v$ a.e. in B_1, which (together with dominated convergence) in turn implies $\nabla v_n \to \nabla v$ in $L^p(B_1)$ for each $p \geq 1$, and $\tilde{v} = v$.

Let us start by observing that, by our preceding considerations, the deformation v_n is explicitly given by (21), and thus

(69)
$$\nabla v_n(x) = \sum_{k=0}^{N_n} R_E R_*^k Q_\alpha^k (\nabla u)(r_I^{-k} Q_{-\alpha}^k x) Q_{-\alpha}^k \chi_{\Sigma_k} + R_E \chi_{\mathbb{R}^2 \setminus \Sigma_0^{co}} + R_E R_*^{N_n+1} \chi_{\overline{\Sigma}_{N_n+1}^{co}},$$

and where ∇u is given by (33). Next we notice that the set

$$\mathcal{Z} := \bigcup_{n=3}^{\infty} \bigcup_{k=0}^{N_n} \bigcup_{i=1}^{n} \Big(\partial(r_I^k Q_\alpha^k Q_{i-1} T_1) \cup \partial(r_I^k Q_\alpha^k Q_{i-1} T_2) \Big),$$

which is the union over all the boundaries of the $2n$ triangles in each of the $N_n + 1$ layers Σ_k, has zero two-dimensional Lebesgue measure. Here, as above, Q_j is a rotation of angle $\frac{2\pi j}{n}$. Let us now fix $x \in B_{\frac{1}{2}} \setminus \mathcal{Z}$. Then, there exists $n_x \geq 3$ such that $x \in B_{\frac{1}{2}} \setminus \bigcup_{k=0}^{N_n} \Sigma_k$ for every $n \geq n_x$. For $n \geq n_x$, then $\nabla v_n(x) = R_E R_*^{N_n}$ and $R_E R_*^{N_n} \to Q(1-2\alpha) Q(\rho_0 \log \frac{1}{2})$ as $n \to \infty$ (see (73) below).

Let now $x \in B_1 \setminus \big(B_{\frac{1}{2}} \cup \mathcal{Z}\big)$. Then, there exists $n_x \geq 3$ such that $x \in \bigcup_{k=0}^{N_n} \Sigma_k$ for every $n \geq n_x$. Therefore, given any $n \geq n_x$ we have that there exists $0 \leq k \leq N_n$ and $1 \leq i \leq n$ such that $x \in r_I^k Q_\alpha^k Q_{i-1} T_1$ or such that $x \in r_I^k Q_\alpha^k Q_{i-1} T_2$. Suppose without loss of generality the first inclusion holds, as the second case can be treated similarly (see (75) below). We then have that

$$\nabla v_n(x) = R_*^k Q_\alpha^k Q_{i-1} H Q_{i-1}^T Q_{-\alpha}^k. \tag{70}$$

Furthermore,

$$|x - r_I^k Q_\alpha^k Q_{i-1} e_1| \leq r_I^k \operatorname{diam} T_1 \leq r_I^k \frac{c_0}{n}, \tag{71}$$

where we denoted by $\operatorname{diam} T_1$ the maximal Euclidean distance between two points within $\overline{T}_1$ (the closure of T_1), which can be bounded by a positive constant c_0 (independent of n, i, k) divided by n. Let now $(r,\omega), (r_0,\omega_0) \in (\frac{1}{2}, 1) \times [0, 2\pi)$ be respectively the polar coordinates of x and $r_I^k Q_\alpha^k Q_{i-1} e_1$. We notice that, by (71),

$$|Q_\alpha^k Q_{i-1} - Q(\omega)| = |Q(\omega_0) - Q(\omega)| \leq \frac{c_1}{n}, \tag{72}$$

for some $c_1 > 0$ independent of i, k, n. On the other hand,

$$k = \frac{\log(r_0)}{\log(r_I)}.$$

Now, as $\log r_I = -\frac{2\pi\sqrt{\alpha(1-\alpha)}}{n} + o(n^{-1})$ as $n \to \infty$, and using the notation that $Q_\varphi = Q(\frac{2\pi}{n}\varphi)$, we obtain that

$$\begin{aligned} R_*^k = Q_{(1-2\alpha)k} &= Q\left(\frac{2\pi}{n}(1-2\alpha) \frac{\log(r_0)}{-\frac{2\pi\sqrt{\alpha(1-\alpha)}}{n} + o(n^{-1})} \right) \\ &\to Q\left(\frac{(2\alpha-1)}{\sqrt{\alpha(1-\alpha)}} \log(r_0) \right) =: Q(\rho_0 \log(r_0)). \end{aligned} \tag{73}$$

Finally, we recall that e_{11} is a normalised version of

$$1-\frac{r_I}{r_E}e^{i\frac{2\pi}{n}\alpha}=1-\left(1-\frac{2\pi}{n}\sqrt{\alpha(1-\alpha)}\right)\left(1+i\frac{2\pi}{n}\alpha\right)+O(n^{-2})$$
$$=\frac{2\pi}{n}(\sqrt{\alpha(1-\alpha)}-i\alpha)+\mathcal{O}(n^{-2}),$$

where we have identified $\mathbb{R}^2$ with $\mathbb{C}$. Normalising and taking the limit, we hence obtain that

$$e_{11}\to\begin{pmatrix}\sqrt{1-\alpha}\\-\sqrt{\alpha}\end{pmatrix}=:\bar{e}_{11}.$$

As a consequence,

$$H\to a\bar{e}_{11}\otimes\bar{e}_{11}+a^{-1}\bar{e}_{11}^{\perp}\otimes\bar{e}_{11}^{\perp}=:H_\infty, \tag{74}$$

where we used that $\frac{1}{\tan\phi}=\frac{1}{\tan(\frac{n-2}{2n}\pi)}\to 0$. We remark that, in the case $x\in r_I^kQ_\alpha^kQ_{i-1}T_2$ for some $n\geq 3$, $0\leq i\leq n$ and some $0\leq k\leq N_n$ the proof differs just for (74) which should read

(75)
$$P_0HP_0\to(\bar{e}_{11}\otimes\bar{e}_{11}-e_{11}^{\perp}\otimes e_{11}^{\perp})(a\bar{e}_{11}\otimes\bar{e}_{11}+a^{-1}\bar{e}_{11}^{\perp}\otimes\bar{e}_{11}^{\perp})(\bar{e}_{11}\otimes\bar{e}_{11}-e_{11}^{\perp}\otimes e_{11}^{\perp})$$
$$=a\bar{e}_{11}\otimes\bar{e}_{11}+a^{-1}\bar{e}_{11}^{\perp}\otimes\bar{e}_{11}^{\perp}=H_\infty.$$

Therefore, collecting (70)–(74), by the triangle inequality we get

$$|\nabla v_n(x)-\nabla v(x)|$$
$$\leq c_2\big(\max\{|H-H_\infty|,|P_0HP_0-H_\infty|\}+|Q_\alpha^kQ_{i-1}-Q(\omega)|$$
$$+|R_*^k-Q(\rho_0\log r_0)|+|Q(\rho_0\log r)-Q(\rho_0\log r_0)|\big)\to 0,$$

for some $c_2>0$. This concludes the proof of the claim. □

Proof of Corollary 4.3. In order to compute the underlying vector field, we note that in polar coordinates

$$x=\begin{pmatrix}r\cos(\omega)\\r\sin(\omega)\end{pmatrix},$$

we have by virtue of the chain rule

$$\begin{pmatrix}\frac{\partial v_j}{\partial x_1}\\\frac{\partial v_j}{\partial x_2}\end{pmatrix}=\begin{pmatrix}\cos(\omega)&-\frac{1}{r}\sin(\omega)\\\sin(\omega)&\frac{1}{r}\cos(\omega)\end{pmatrix}\begin{pmatrix}\frac{\partial\hat{v}_j}{\partial r}\\\frac{\partial\hat{v}_j}{\partial\omega}\end{pmatrix},$$

where $\hat{v}_j(r,\omega)=v_j(r\cos(\omega),r\sin(\omega))$ and $j\in\{1,2\}$. As a consequence,

$$\begin{pmatrix}\frac{\partial\hat{v}_j}{\partial r}\\\frac{\partial\hat{v}_j}{\partial\omega}\end{pmatrix}=r\begin{pmatrix}\frac{1}{r}\cos(\omega)&\frac{1}{r}\sin(\omega)\\-\sin(\omega)&\cos(\omega)\end{pmatrix}\begin{pmatrix}\frac{\partial v_j}{\partial x_1}\\\frac{\partial v_j}{\partial x_2}\end{pmatrix}=F(r,\omega)M(\omega)Q(-\rho_0\log(r))e_j,$$

where

$$F(r,\omega)=r\begin{pmatrix}\frac{1}{r}\cos(\omega)&\frac{1}{r}\sin(\omega)\\-\sin(\omega)&\cos(\omega)\end{pmatrix},$$
$$M(\omega)=Q(\omega)(a\bar{e}_{11}\otimes\bar{e}_{11}+a^{-1}\bar{e}_{11}^{\perp}\otimes\bar{e}_{11}^{\perp})^TQ(-\omega).$$

Simplifying the corresponding expressions, we obtain

$$\begin{pmatrix} \frac{\partial \hat{v}_1}{\partial r} \\ \frac{\partial \hat{v}_1}{\partial \omega} \end{pmatrix} = \begin{pmatrix} \frac{1+2\alpha(\alpha-1)}{\sqrt{\alpha(1-\alpha)}} \cos(\omega + \rho_0 \log(r)) + (1-2\alpha)\sin(\omega + \rho_0 \log(r)) \\ r\left((-1+2\alpha)\cos(\omega + \rho_0 \log(r)) - 2\sqrt{\alpha(1-\alpha)}\sin(\omega + \rho_0 \log(r))\right) \end{pmatrix},$$

$$\begin{pmatrix} \frac{\partial \hat{v}_2}{\partial r} \\ \frac{\partial \hat{v}_2}{\partial \omega} \end{pmatrix} = \begin{pmatrix} (-1+2\alpha)\cos(\omega + \rho_0 \log(r)) + \frac{1+2\alpha(\alpha-1)}{\sqrt{1-\alpha}}\sin(\omega + \rho_0 \log(r)) \\ r\left(2\sqrt{(1-\alpha)\alpha}\cos(\omega + \rho_0 \log(r)) + (-1+2\alpha)\sin(\omega + \rho_0 \log(r))\right) \end{pmatrix}.$$

Integrating these expressions (in particular the ω integration becomes quite straight forward) then yields the desired result. □

Proof of Lemma 4.4. The convergence of $K_n(a)$ to $K_\infty(a)$ follows from the pointwise convergence of $H(a)$ to the matrix $H_\infty(a)$ as $n \to \infty$ (see (74)) and the fact that $\mathcal{P}_n \to O(2)$ as $n \to \infty$.

In order to observe the claimed identity, we note that by the properties of the determinant and of $H_\infty(a)$, it holds

$$\bigcup_{P \in O(2)} SO(2) P H_\infty(a) P^T \subset \{F \in \mathbb{R}^{2\times 2} : \ \det(F) = 1, \ \lambda(F) = a, \ \mu(F) = a^{-1}\}$$
$$=: K'_\infty(a).$$

It hence remains to prove the reverse inclusion. Let $F \in K'_\infty(a)$. Then, by the polar decomposition $F = R_1 V$ for some $R_1 \in SO(2)$ and some $V \in \mathbb{R}^{2\times 2}$ symmetric, positive definite with eigenvalues a, a^{-1}. Now, by the spectral theorem and the fact that H_∞ is diagonal, there exists $R_2 \in SO(2)$ such that $R_2 H_\infty R_2^T = V$. As a consequence, $F = R_1 R_2 H_\infty R_2^T$, which concludes the proof.

The identity for ∇v follows directly from Proposition 4.1. □

4.3. **The limit $n \to \infty$ in the geometrically linearised setting.** Similarly as in Section 4.1 in the geometrically non-linear set-up, also in the geometrically linearised setting we now consider the limit $n \to \infty$. In particular, we are then naturally lead to the same deformation as the one discussed in [ADMD15] in the context of nematic liquid crystal elastomers.

Lemma 4.5. *For $n \to \infty$, the set K from (61) turns into*

$$K_\infty := \left\{ R \begin{pmatrix} 1 & 0 \\ 0 & -1 \end{pmatrix} R^T : \ R \in O(2), \ c \in \mathbb{R} \right\}$$
$$= \left\{ c \begin{pmatrix} a & b \\ b & -a \end{pmatrix} : \ a^2 + b^2 = 1, \ c = \frac{1}{\sin(\frac{\pi}{n})} \right\}.$$

Proof. The first identity follows from considering $n \to \infty$ in (58). The second identity is a consequence of the explicit form of $O(2)$. □

As a consequence, the differential inclusion which we study turns into

$$e(\nabla u) \in K_\infty. \tag{76}$$

Linearising the solution from Proposition 4.1, we obtain a two-dimensional solution to the differential inclusion (76) with zero boundary conditions:

Proposition 4.6. *The function*

$$w(x) = 2(1 - \log(r^2))(x_2, -x_1)$$

is a solution to the differential inclusion (76) in $B_1 \setminus \overline{B_{1/2}}$ and $\nabla u = 0$ in $\mathbb{R}^n \setminus \overline{B_1}$.

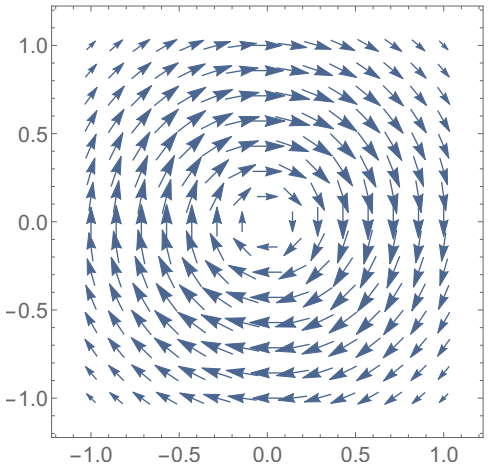

FIGURE 11. A plot of the vector field $w(x)$ from Proposition 4.6.

Proof. The claim follows from the identity

$$w(x_1, x_2) := \frac{d}{d\alpha} v_\alpha(x_1, x_2)|_{\alpha=\frac{1}{2}},$$

where v_α denotes the family of solutions from Proposition 4.1 with $\alpha \in (0,1)$, the differential inclusion which is solved by v_α and the linearisation arguments from above. Indeed, a computation shows that

$$\begin{aligned}
\frac{d}{d\alpha} v_\alpha(x_1, x_2)\big|_{\alpha=\frac{1}{2}} &= rQ'(\omega + \rho_0|_{\alpha=\frac{1}{2}})\rho_0'|_{\alpha=\frac{1}{2}} \log(r) \begin{pmatrix} 1 \\ 0 \end{pmatrix} \\
&\quad + rQ(\omega + \rho_0|_{\alpha=\frac{1}{2}} \log(r)) \begin{pmatrix} 0 \\ -2 \end{pmatrix} \\
&= 4rQ'(\omega) \log(r) \begin{pmatrix} 1 \\ 0 \end{pmatrix} + rQ(\omega) \begin{pmatrix} 0 \\ -2 \end{pmatrix} \\
&= 2(1 - \log(r^2)) \begin{pmatrix} x_2 \\ -x_1 \end{pmatrix}.
\end{aligned}$$

Here $Q'(\omega)$ denotes the derivative of $Q(\omega)$ with respect to ω. □

Remark 4.7. *We note that up to a multiplicative constant and an affine off-set whose gradient is a skew matrix, the function $w(x)$ recovers the special solution from Theorem 2.1 in* [ADMD15]. *This was found in* [ADMD15] *in the context of convex integration solutions for differential inclusions in nematic liquid crystal elastomers. In the next section, we establish the connection between the differential inclusion* (76) *and the one associated with two-dimensional liquid crystal elastomers.*

Last but not least, we recall the modelling of nematic liquid crystal elastomers within the geometrically linearised theory and relate the associated differential inclusion for planar deformation to the differential inclusions, which we have considered in the previous section.

A prominent class of stored energy densities in the modelling of nematic liquid crystal elastomers within the geometrically linearised theory (which can formally be obtained as the linearisation of the non-linear energies) is of the form

$$V(E) = \min_{\hat{n} \in S^2} |E - H_{\hat{n}}|^2, \; H_{\hat{n}} = \frac{1}{2}(3\hat{n} \otimes \hat{n} - I), \tag{77}$$

where $E \in \mathbb{R}^{3\times 3}_{sym}$ and $\mathrm{tr}(E) = 0$, see [Ces10]. Seeking to study energy zero solutions, one is thus lead to the corresponding differential inclusion problem

$$e(\nabla u) \in K_{3D} := \{E \in \mathbb{R}^{3\times 3}_{sym};\ \mu_1(E) = \mu_2(E) = -\frac{1}{2},\ \mu_3(E) = 1\}, \tag{78}$$

where $\mu_j(E)$ denote the ordered eigenvalues of E. We note that for affine boundary conditions, the relaxation of this differential inclusion is given by

$$e(\nabla u) \in K_{3D},\ \nabla u = M \text{ for some } M \in K^{qc}_{3D}, \tag{79}$$

where

$$K^{qc}_{3D} = \{E \in \mathbb{R}^{3\times 3}_{sym} :\ -\frac{1}{2} \le \mu_1(E) \le \mu_2(E) \le \mu_3(E) \le 1,\ \mathrm{tr}(E) = 0\}. \tag{80}$$

We refer for this to [ADMD15], and also to Chapter 7 in [DM12].

An interesting class of deformations is given by planar deformations. These were for instance studied in [CD11]. In searching for energy zero solutions to (77) with microstructure only in the planar direction, we study the following displacements

$$v(x_1, x_2, x_3) = (\tilde{v}(x_1, x_2), 0) + \left[\begin{pmatrix} M' & 0 \\ 0 & m_{33} \end{pmatrix} x\right]^T,$$

where $M \in \mathbb{R}^{2\times 2}$ and where $\tilde{v}(x_1, x_2) = 0$ on ∂B_1, i.e. where the boundary data are encoded in the matrix $M = \begin{pmatrix} M' & 0 \\ 0 & m_{33} \end{pmatrix}$. In order to both ensure that v is a solution to the differential inclusion (79) and that there is interesting microstructure in the problem, we set $m_{33} = -\frac{1}{2}$ and consider boundary data M which are of the form $M = \begin{pmatrix} M' & 0 \\ 0 & -\frac{1}{2} \end{pmatrix}$. For the resulting two-dimensional displacement $\tilde{v}$ one is then lead to the following differential inclusion:

$$e(\nabla \tilde{v} + M') \in K_{2D} := \left\{E \in \mathbb{R}^{2\times 2}_{sym} :\ -\frac{1}{2} = \mu_1(E) < \mu_2(E) = 1;\ \mathrm{tr}(E) = \frac{1}{2}\right\}. \tag{81}$$

The (relaxed) condition for M' turns into

$$e(M') \in \mathrm{int}(K^{qc}_{2D}) := \left\{E \in \mathbb{R}^{2\times 2}_{sym} :\ -\frac{1}{2} < \mu_1(E) \le \mu_2(E) < 1;\ \mathrm{tr}(E) = \frac{1}{2}\right\}. \tag{82}$$

We are now searching for a solution $\tilde{v}(x_1, x_2)$ satisfying (81), (82) such that $\tilde{v}(x_1, x_2) = 0$ on ∂B_1. To this end, we note the following necessary and sufficient conditions:

Lemma 4.8. *Let $\tilde{v}(x_1, x_2)$ be a solution to*

$$e(\nabla \tilde{v} + M') \in K_{2D} \text{ in } B_1,\ \tilde{v} = 0 \text{ on } \partial B_1. \tag{83}$$

Then, a necessary and sufficient condition for (83) is that

$$\left(\partial_1 \tilde{v}_1 + e_{11}(M') - \frac{1}{4}\right)^2 + \left(\frac{1}{2}(\partial_1 \tilde{v}_2 + \partial_2 \tilde{v}_1) + e_{12}(M')\right)^2 = \frac{9}{16}. \tag{84}$$

Remark 4.9. *By using the trace constraints from (82) and (81), we can rewrite*

$$e(M') = \begin{pmatrix} e_{11}(M') & e_{12}(M') \\ e_{12}(M') & -e_{11}(M') + \frac{1}{2} \end{pmatrix},\ e(\nabla \tilde{v}) = \begin{pmatrix} \partial_1 \tilde{v}_1 & \frac{1}{2}(\partial_1 \tilde{v}_2 + \partial_2 \tilde{v}_1) \\ \frac{1}{2}(\partial_1 \tilde{v}_2 + \partial_2 \tilde{v}_1) & \partial_2 \tilde{v}_2 \end{pmatrix}, \tag{85}$$

with $\partial_2\tilde{v}_2 = -\partial_1\tilde{v}_1$. *The differential inclusion* (84) *can then be written in a more symmetric form:*

$$\begin{aligned}(86)\qquad &\frac{1}{2}\left(\partial_2\tilde{v}_2 + e_{22}(M') - \frac{1}{4}\right)^2 + \frac{1}{2}\left(\partial_1\tilde{v}_1 + e_{11}(M') - \frac{1}{4}\right)^2 \\ &+ \left(\frac{1}{2}(\partial_1\tilde{v}_2 + \partial_2\tilde{v}_1) + e_{12}(M')\right)^2 = \frac{9}{16}.\end{aligned}$$

For $e_{11}(M') = \frac{1}{4}$, $e_{12}(M') = 0$ *and* $e_{22}(M') = \frac{1}{4}$ *equation* (86) *hence resembles a vectorial Eikonal type equation.*

Remark 4.10. *As a further observation, which might also be of interest in the context of the (quantitative) investigation of convex integration solutions, we point out that the setting of geometrically linear liquid crystal problems fits into the framework of* [RZZ18]. *As a consequence, it is possible to deduce the existence of "wild" solutions with higher regularity. This is a consequence of the structure of the set* K^{qc} *from* (80) *for which appropriate in-approximations and replacement constructions can be found similarly as in the* $O(n)$ *case.*

Proof. Necessity: By definition of the set K_{2D}, for all matrices $\tilde{E} \in K_{2D}$ it holds that $\det(\tilde{E}) = \frac{1}{2}$. Hence, a necessary condition for (83) is clearly given by the requirement that

$$\det(e(\nabla\tilde{v} + M')) = -\frac{1}{2}.$$

With a few computations, it can be observed that this is equivalent to (84).

Sufficiency: A sufficient requirement for the validity of (83) is that

$$\det(e(\nabla\tilde{v}) + M' - \lambda Id) = 0 \tag{87}$$

for $\lambda = 1$ and $\lambda = \frac{1}{2}$. Equation (87) can be rewritten as

$$\lambda^2 - \frac{\lambda}{2} + \det(e(\nabla\tilde{v}) + M') = 0.$$

Simplifying this expression for the choice $\lambda = 1$ and $\lambda = \frac{1}{2}$ then indeed also leads to (84). □

With Lemma 4.8 in hand, we can relate the differential inclusion from (76) to the nematic liquid crystal elastomer differential inclusions (83), (84). This allows us to "explain" the coincidence of the solution from Proposition 4.6 and the one found in [ADMD15]:

Corollary 4.11. *Let* v *be the solution from Proposition 4.6. Then,* $\frac{4}{3}v$ *is a solution to* (86) *with*

$$e(M') = \begin{pmatrix} \frac{1}{4} & 0 \\ 0 & \frac{1}{4} \end{pmatrix}.$$

Proof. The result follows directly by comparing the form of K_∞ from Lemma 4.5 and (84). For the chosen value of $e(M')$ the differential inclusions only differ by a multiplicative constant. □

5. Remarks on Three-Dimensional Constructions

Last but not least, in this final section before the appendix we discuss adaptations of the two-dimensional constructions of Section 2.1 to the case of two nested regular tetrahedra $T_1, T_2 \subset \mathbb{R}^3$. Here, it turns out that while it is possible to construct

families of volume-preserving piecewise affine transformations, there are no non-trivial constructions which exhibit an m-well structure

$$\nabla u \in SO(3) \cup \bigcup_{P \in \mathcal{P}_n} SO(3) P U P^T; \ \det(U) = 1, \tag{88}$$

where $\nabla u \in SO(3)$ corresponds to an austenite configuration and $\mathcal{P}_n \subset SO(3)$ denotes a suitable symmetry group.

After possibly rescaling and rotating u, we may assume that T_1 is given by the convex hull of the four points

$$\begin{pmatrix} 1 \\ 1 \\ 1 \end{pmatrix}, \begin{pmatrix} 1 \\ -1 \\ -1 \end{pmatrix}, \begin{pmatrix} -1 \\ 1 \\ -1 \end{pmatrix}, \begin{pmatrix} -1 \\ -1 \\ 1 \end{pmatrix}. \tag{89}$$

With this choice of coordinates, the barycenter of T_1 is in $(0,0,0)$ and two distinguished axes of rotation are given by the x_3 axis

$$\mathbb{R} \begin{pmatrix} 0 \\ 0 \\ 1 \end{pmatrix} \tag{90}$$

and

$$\mathbb{R} \begin{pmatrix} 1 \\ 1 \\ 1 \end{pmatrix} \tag{91}$$

Furthermore, the dual tetrahedron to T_1 is up to rescaling given by $-T_1$.

In the following we consider two symmetric constructions, where the inner tetrahedron T_2 has the same barycenter and shares an axis of symmetry with T_1. The deformation u is then obtained by rotating T_2 around this axis and linearly interpolating on the polyhedra spanned by vertices, edges and surfaces of T_1 and T_2. By our choice of coordinates we may assume that the distinguished axis is either given by (90) which is illustrated in Figures 12 and 13, or by (91) which is illustrated in Figures 14 and 15.

In particular, since u is required to be volume-preserving as $K \subset \{M : \det(M) = 1\}$, it follows that u needs to preserve the distance of the vertices of T_2 to the corresponding surfaces of T_1. Computations show that there is no non-trivial choice of T_2 and RT_2 such that this distance is the distance for all four corners of T_2. Hence, we relax this constraint to consider the case where T_2 is chosen to be a rescaled dual copy of T_1, which is initially rotated around either $\mathbb{R} \begin{pmatrix} 1 \\ 1 \\ 1 \end{pmatrix}$ or the x_3-axis. These configurations are depicted in Figure 12 and Figure 14, respectively.

5.1. **Rotations around the x_3-axis.** We first consider the setting depicted in Figures 12 and 13. We in particular note that the cyan interpolation region (for colours we refer to the online version of the article) is obtained by interpolating between a surface S of T_1 and a vertex v of T_2. The volume-preservation constraint $\det(\nabla u) = 1$ imposed by the m-well condition (88) thus implies that the map u needs to preserve the distance between the surface $S = u(S)$ and $u(v)$. Similarly to the two-dimensional setting (c.f. Figure 3 and the preceding remarks) this implies that if initially

$$T_2 = rR_{-\theta}(-T_1), \tag{92}$$

then necessarily

$$u(T_2) = rR_{+\theta}(-T_1), \tag{93}$$

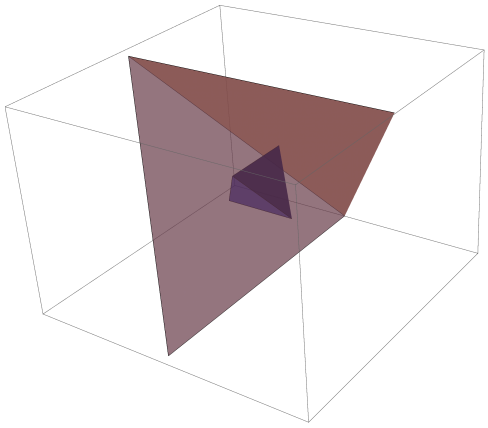

FIGURE 12. The inner tetrahedron T_2 shares the x_3-axis as a common symmetry axis with T_1. Upon rotating T_2 around this axis, a piecewise affine transformation u is obtained by interpolating on the various polyhedra shown in Figure 13.

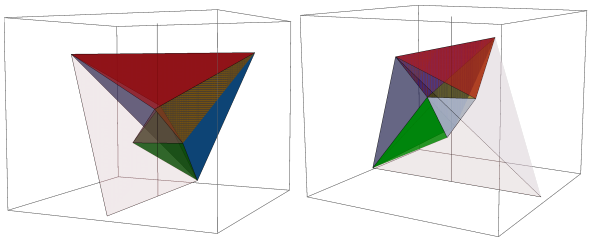

FIGURE 13. The inner and outer tetrahedron both share the x_3 axis as a symmetry axis, viewed here from two different rotated points of view. We consider a map u, which is affine in the interior tetrahedron, given by the identity outside the outer tetrahedron and given by affine interpolations in the remaining regions composed of (irregular) tetrahedra. Up to symmetry, there are 5 distinct interpolation regions, which are coloured in this picture.

where $r \in (1, \frac{1}{3})$ is a scaling factor, R_θ is the rotation around the x_3 axis with angle θ and we recall that, up to scaling, $-T_1$ is the dual tetrahedron to T_1. Thus u acts on T_2 by a rotation by 2θ and we say that the tetrahedron is "flipped" from being rotated by an angle $-\theta$ to being rotated by an angle θ. With this choice, for any $r > 0$ and any $\theta > 0$, it follows that u is a volume preserving affine transformation in each of the regions highlighted in Figure 13. However, while volume-preservation is a necessary condition for the m-well problem (88), this is not sufficient. We may explicitly compute that in the red interpolation region ∇u is given by the shear

$$U_1(\theta) = \begin{pmatrix} 1 & 0 & 0 \\ 2\tan(\theta) & 0 & 0 \\ 0 & 0 & 1 \end{pmatrix}, \tag{94}$$

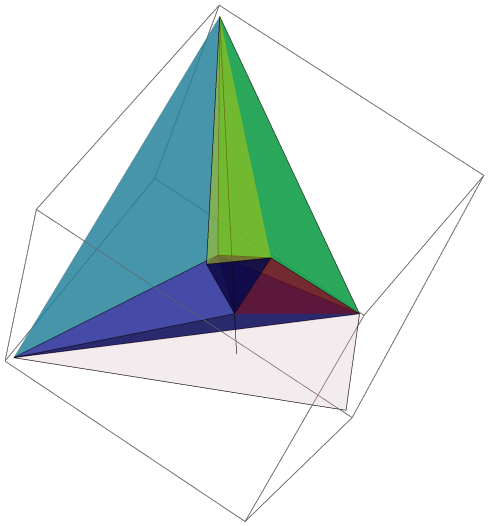

FIGURE 14. The tetrahedra share a common symmetry axis through their barycenter and one of the corners. We consider a map u, which is given by a rotation in the interior tetrahedron, by the identity outside the outer tetrahedron and given by affine interpolations in the remaining regions composed of (irregular) tetrahedra. Up to symmetry, there are 5 distinct interpolation regions, which are coloured in this picture.

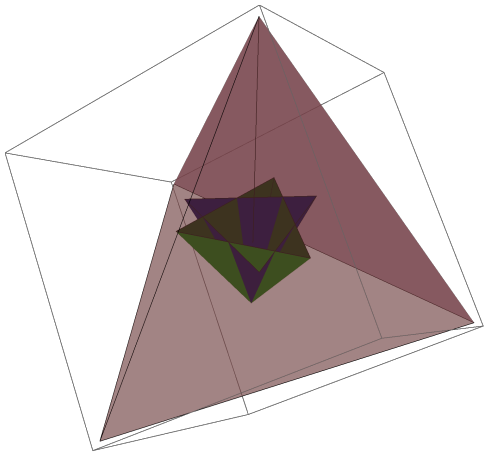

FIGURE 15. Given an initial configuration depicted in blue, the green "flipped" configuration is the only rotation around the symmetry axis that preserves the volume of the polyhedra spanned by an inner corner and an outer surface.

and in particular is independent of $r > 0$. Since none of the interpolated transformations are given by rotations, we thus ask whether there exist suitable choices of θ, r such that

$$\nabla u \in \bigcup_{P \in \mathcal{P}_n} SO(3) P U_1 P^T \tag{95}$$

in the remaining regions for a suitable choice of a symmetry group $\mathcal{P}_n$. A necessary condition for this requirement is that in all interpolation regions the singular values of ∇u agree with the singular values of U_1. An explicit numerical computation yields that the singular values are given by $(\lambda, 1, \frac{1}{\lambda})$, where λ depends on the angle θ and the scaling factor r chosen in (92) and the interpolation region.

Figure 16 shows plots of λ in the various regions and was obtained by direct numerical calculations.

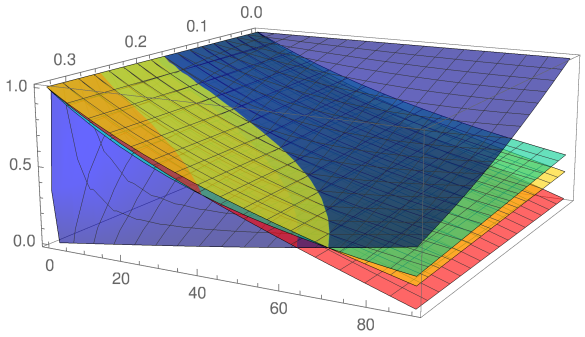

FIGURE 16. Singular values for the construction of Figure 13. We numerically compute the smallest singular value of the transformation u in various regions as functions of the angle $\theta \in (0, \frac{\pi}{2})$ and scaling factor $r \in (0, \frac{1}{3})$ chosen in (92).

In particular, we observe that there are no non-trivial choices of r, θ such that the singular values λ agree in all regions. The necessary condition for the m-well inclusion (95) is thus never satisfied.

We remark that key obstacles of this three-dimensional construction are given by the non-commutative structure of $SO(3)$ and the requirement to choose an axis for the rotation of T_2. While in two dimensions all rotations commute and all interpolation regions are given by triangles, in the present setting the interpolations in the various regions instead behave qualitatively differently and are for instance not anymore given by shears.

5.2. **Rotations around an axis through a vertex.** In this subsection we consider the construction depicted in Figure 14, where

$$T_2 = rR^*_{-\theta}(-T_1), \tag{96}$$

is instead rotated around the axis (91) through the origin and one of the corners of T_1. As in the two-dimensional case, the determinant constraint and the resulting volume preservation implies that an inner tetrahedron initially rotated by an angle $-\theta$ compared to the dual tetrahedron of T_1 can only be "flipped" to an angle θ (see Figure 15 for an illustration):

$$u(T_2) = rR^*_{-\theta}(-T_1). \tag{97}$$

We thus consider the mapping $u : \mathbb{R}^3 \to \mathbb{R}^3$ which acts as the identity outside the outer tetrahedron T_1, as a rotation by 2θ around the symmetry axis inside T_2, and is given by the affine interpolation in any of the (irregular) tetrahedra of the types depicted in Figure 14. With this choice of construction the transformation

u is volume-preserving on all interpolation regions for all choices of $r \in (0, \frac{1}{3})$ and $\theta \in (-\frac{\pi}{2}, \frac{\pi}{2})$. As a main difference to the construction of Section 5.1 for the x_3-axis case, we observe that under this transformation, the tetrahedron obtained by interpolating between a surface of T_2 and $(1,1,1)$ (coloured yellow in Figure 14) is transformed by a rigid rotation and thus corresponds to austenite. Furthermore, the region obtained by interpolating between a surface of T_1 and the vertex $-r(1,1,1) \in T_2$ remains invariant under u and thus also corresponds to austenite. For the remaining regions, we thus ask whether there is a choice of parameters $r \in (0, \frac{1}{3}), \theta \in (-\frac{\pi}{2}, \frac{\pi}{2})$ and a suitable matrix U and group $\mathcal{P}_n \subset SO(3)$ such that

$$\nabla u \in \bigcup_{P \in \mathcal{P}_n} SO(3) P U P^T. \tag{98}$$

As in the setting of Subsection 5.1 the singular values in these regions are given by $\lambda, 1, \frac{1}{\lambda}$.

A plot of λ in the various regions obtained by direct numerical computation is given in Figure 17. In particular, we again observe that there are no non-trivial choices of r, θ such that the singular values λ agree in all regions. The necessary condition for the m-well inclusion (98) is thus never satisfied.

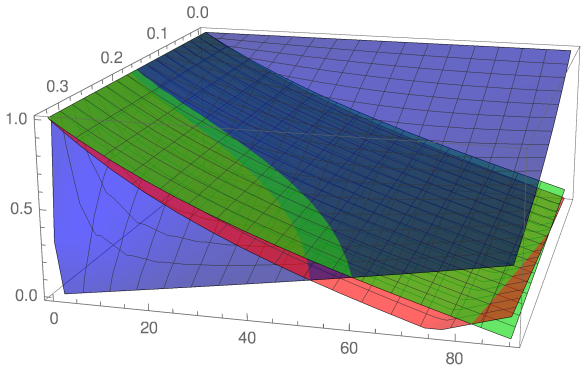

FIGURE 17. Singular values for the construction of Figure 14. We numerically compute the smallest singular value of the transformation u in various regions as functions of the angle $\theta \in (0, \frac{\pi}{2})$ and scaling factor $r \in (0, \frac{1}{3})$ chosen in (96).

APPENDIX A. NECESSARY RELATION BETWEEN THE RADIUS OF THE OUTER POLYGON AND THE RADIUS OF THE INNER POLYGON: THE SOLUTIONS TO (31)

In this first part of the appendix, we provide the remainder of the argument from Proposition 1.

To this end, we solve

$$\begin{aligned}\Big(1 + x^2 - 2x\cos\big(\frac{2\pi}{n}\alpha\big)\Big)\Big(1 + x^2 - 2x\cos\Big(\frac{2\pi}{n}(1-\alpha)\Big)\Big)\cos\Big(\frac{(n-2)\pi}{2n}\Big) \\ = \Big(1 + x^2\cos\big(\frac{2\pi}{n}\big) - 2x\cos\big(\frac{\pi}{n}\big)\cos\big(\frac{\pi}{n}(1-2\alpha)\big)\Big)^2\end{aligned} \tag{99}$$

which is (31) squared. We get the following four solutions of the equation (31) for x:

- $x = \frac{1}{\cos\frac{\pi}{n}}\left(\cos\left(\frac{\rho_n}{2}\right) - \sqrt{\sin(\frac{2\pi}{n}\alpha)\sin\left(\frac{2\pi}{n}(1-\alpha)\right)}\right)$,
- $x = \frac{1}{\cos\frac{\pi}{n}}\left(\cos\left(\frac{\rho_n}{2}\right) + \sqrt{\sin(\frac{2\pi}{n}\alpha)\sin\left(\frac{2\pi}{n}(1-\alpha)\right)}\right)$,
- $x = \frac{1}{\cos\left(\frac{3\pi}{n}\right)}\left(\cos\left(\frac{2\pi}{n}\right)\cos\left(\frac{\rho_n}{2}\right) - \sqrt{\cos^2\left(\frac{2\pi}{n}\right)\cos^2\left(\frac{\rho_n}{2}\right) - \cos\left(\frac{3\pi}{n}\right)\cos\left(\frac{\pi}{n}\right)}\right)$,
- $x = \frac{1}{\cos\left(\frac{3\pi}{n}\right)}\left(\cos\left(\frac{2\pi}{n}\right)\cos\left(\frac{\rho_n}{2}\right) + \sqrt{\cos^2\left(\frac{2\pi}{n}\right)\cos^2\left(\frac{\rho_n}{2}\right) - \cos\left(\frac{3\pi}{n}\right)\cos\left(\frac{\pi}{n}\right)}\right)$,

where as in (iv), $\rho_n := \frac{2\pi}{n}(1-2\alpha)$. We now claim that just the first solution is admissible for us. Here and below we define a solution x of (99) admissible if $x \in (0,1)$ and it satisfies (31). In order to prove our claim, we can assume without loss of generality that

$$\sqrt{4\cos^2\left(\frac{2\pi}{n}\right)\cos^2\left(\frac{\rho_n}{2}\right) - 4\cos\left(\frac{3\pi}{n}\right)\cos\left(\frac{\pi}{n}\right)}$$

is real, otherwise the third and fourth solutions are not admissible. The proof of the claim is as follows:

- Second solution: We estimate

$$x \geq \frac{\cos\left(\frac{\rho_n}{2}\right)}{\cos\left(\frac{\pi}{n}\right)}.$$

  Since $\alpha \in (0,1)$ it is clear that the second solution is such that $x \geq 1$ for any $\alpha \in (0,1)$, any $n \geq 3$.
- Third solution: $x \geq 1$ if $n = 3, 4$ and $\alpha \in [0,1]$. We can hence restrict to the case $n > 4$. We now claim that

$$1 + x^2\cos(\frac{2\pi}{n}) - 2x\cos(\frac{\pi}{n})\cos(\frac{\rho_n}{2}) < 0 \tag{100}$$

  for any $\alpha \in (0,1)$, and any $n \geq 4$. Since the left-hand side of (31) is always non-negative, the claim would imply that the third solution of (99) does not satisfy (31), and is hence not admissible. We plot $1 + x^2\cos(\frac{2\pi}{n}) - 2x\cos(\frac{\pi}{n})\cos(\frac{\rho_n}{2})$ for $n \in \{5, \ldots, 50\}$ in Figure 18. For large n, we have that

$$x = 1 - \frac{2\pi}{n}\sqrt{(\alpha - \alpha^2)} + \frac{2\pi^2}{n^2}(-\alpha^2 + \alpha + 1) + O(n^{-3}),$$

  and, therefore,

$$1 + x^2\cos(\frac{2\pi}{n}) - 2x\cos(\frac{\pi}{n})\cos(\frac{\rho_n}{2}) = -\frac{4\pi^3}{n^3}\sqrt{\alpha(1-\alpha)} + O(n^{-4}) < 0$$

  for any $\alpha \in (0,1)$, and for any n large enough.
- Fourth solution: It is easy to see that it is negative for any $\alpha \in [0,1]$ when $n = 3, 4, 5$. Indeed, $\cos\frac{3\pi}{n} < 0$. If $n = 6$ we get $x = \infty$, while for $n > 6$ we have $x > 1$. Indeed, in this case,

$$x \geq \frac{2\cos\left(\frac{2\pi}{n}\right)\cos\left(\frac{\rho_n}{2}\right)}{2\cos\left(\frac{3\pi}{n}\right)} \geq \frac{\cos\left(\frac{2\pi}{n}\right)\cos\left(\frac{\pi}{n}\right)}{\cos\left(\frac{3\pi}{n}\right)} = \frac{1}{2}\left(1 + \frac{1}{2\cos\left(\frac{2\pi}{n}\right) - 1}\right) > 1.$$

  Therefore, for any $\alpha \in [0,1]$ and any $n \geq 3$ the fourth solution is not admissible.

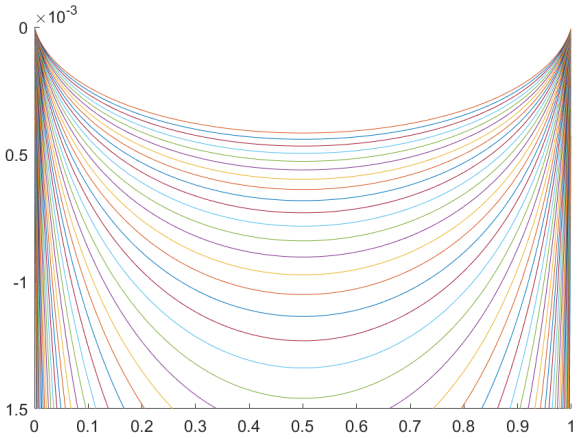

FIGURE 18. Numerical verification of the fact that, for $n \in \{1, \dots, 50\}$ and $\alpha \in (0,1)$ we have (100). The bigger n is, the closer to zero the convex curves in the pictures are.

APPENDIX B. PROOF OF COROLLARY 2.4

In this part of the appendix we show that equation (43)

$$P_0 H P_0 = Q_\alpha H Q_{1-\alpha}^T$$

is satisfied. In order to simplify calculations, we express all matrices with respect to the basis $(e_{11}, e_{11}^\perp)$ and thus have to show that

$$\begin{pmatrix} a & -\frac{a^{-1}-a}{\tan(\phi)} \\ 0 & a^{-1} \end{pmatrix} Q_{1-\alpha} = Q_\alpha \begin{pmatrix} a & \frac{a^{-1}-a}{\tan(\phi)} \\ 0 & a^{-1} \end{pmatrix}. \tag{101}$$

We further recall that

$$a^2 = \frac{\sin(\frac{2\pi}{n}(1-\alpha))}{\sin(\frac{2\pi}{n}\alpha)}, \quad \frac{1}{\tan(\phi)} = \tan\left(\frac{\pi}{n}\right).$$

In particular, since $\alpha \in (0,1)$, we may multiply the claimed equation with $a \sin(\frac{2\pi}{n}\alpha) \neq 0$ and for simplicity of notation introduce $t := \frac{2\pi}{n}\alpha$ and $s = \frac{2\pi}{n}(1-\alpha) = \frac{2\pi}{n} - t$. With this notation, we have to show that

$$\begin{aligned} &\begin{pmatrix} \sin(s) & -(\sin(t)-\sin(s))\tan(\frac{\pi}{n}) \\ 0 & \sin(t) \end{pmatrix} \begin{pmatrix} \cos(s) & -\sin(s) \\ \sin(s) & \cos(s) \end{pmatrix} \\ &= \begin{pmatrix} \cos(t) & -\sin(t) \\ \sin(t) & \cos(t) \end{pmatrix} \begin{pmatrix} \sin(s) & (\sin(t)-\sin(s))\tan(\frac{\pi}{n}) \\ 0 & \sin(t) \end{pmatrix}. \end{aligned}$$

We consider each matrix entry separately. The claimed equality for the upper left entry is given by

$$\sin(s)\cos(s) - \sin(s)\tan\left(\frac{\pi}{n}\right)(\sin(t)-\sin(s)) = \cos(t)\sin(s). \tag{102}$$

In order to show this, we may factor out $\sin(s)$ and use the angle addition formulas:

$$\begin{aligned} \cos(s) &= \cos(t)\cos\left(\frac{2\pi}{n}\right) + \sin(t)\sin\left(\frac{2\pi}{n}\right), \\ \sin(s) &= \cos(t)\sin\left(\frac{2\pi}{n}\right) - \sin(t)\cos\left(\frac{2\pi}{n}\right). \end{aligned}$$

We then collect terms involving $\cos(t)$ and $\sin(t)$ as

$$\begin{aligned}
&\cos(t)\cos\left(\frac{2\pi}{n}\right)+\sin(t)\sin\left(\frac{2\pi}{n}\right)\\
&-\tan\left(\frac{\pi}{n}\right)\left(\sin(t)-\cos(t)\sin\left(\frac{2\pi}{n}\right)+\sin(t)\cos\left(\frac{2\pi}{n}\right)\right)\\
&=\cos(t)\left(\cos\left(\frac{2\pi}{n}\right)+\tan\left(\frac{\pi}{n}\right)\sin\left(\frac{2\pi}{n}\right)\right)\\
&+\sin(t)\left(\sin\left(\frac{2\pi}{n}\right)-\tan\left(\frac{\pi}{n}\right)\left(1+\cos\left(\frac{2\pi}{n}\right)\right)\right)\\
&=\cos(t)1+\sin(t)0=\cos(t),
\end{aligned}$$

where we used the half angle identities for $\cos(2x)$ and $\sin(2x)$ in the last equality.

The calculation for the bottom right-entry is analogous with the role of s and t and the sign of $(\sin(t)-\sin(s))\tan(\frac{\pi}{n}))$ interchanged. The bottom left equality $\sin(t)\sin(s)=\sin(t)\sin(s)$ is always satisfied. It thus only remains to verify equality of the upper right entry, which can be simplified to read

$$\begin{aligned}
&-\sin^2(s)-\cos(s)(\sin(t)-\sin(s))\tan\left(\frac{\pi}{n}\right)\\
&\quad=-\sin^2(t)+\cos(t)(\sin(t)-\sin(s))\tan\left(\frac{\pi}{n}\right)\\
&\Leftrightarrow \sin^2(t)-\sin^2(s)-(\cos(t)+\cos(s))(\sin(t)-\sin(s))\tan\left(\frac{\pi}{n}\right)=0.
\end{aligned}$$

Factoring out the factor $(\sin(t)-\sin(s))$, it suffices to prove

$$\sin(t)+\sin(s)-(\cos(t)+\cos(s))\tan\left(\frac{\pi}{n}\right)=0.$$

As above, the claimed equality then again follows by using angle addition formulas.

Appendix C. Reduction to Cauchy-Green Tensors used in the Proof of Proposition 2.6

Last but not least, we provide the argument (used in the proof of Proposition 2.6) that it is possible to reduce the differential inclusion (23) to an inclusion for the associated Cauchy-Green tensors.

Lemma C.1. *Suppose that* $\det(M)=\det(H)>0$*, then the inclusion*

$$M\in\bigcup_{P\in\mathcal{P}_n} SO(2)P^THP \tag{103}$$

is satisfied, if and only if

$$M^TM\in\bigcup_{P\in\mathcal{P}_n} P^TH^THP. \tag{104}$$

This characterisation follows from basic properties of the singular value decomposition.

Proof. We observe that (103) implies (104). Thus, we only consider the converse and assume that

$$M^TM=(P^TH^TP)(P^THP)=:M_1^TM_1.$$

for some $P\in\mathcal{P}_n$. Since M^TM is symmetric, there exists $Q\in SO(2)$ and a diagonal matrix $\operatorname{diag}(\lambda_1,\lambda_2)$, with $\lambda_1\lambda_2=\det(M)^2\neq 0$, $\lambda_1,\lambda_2>0$, such that

$$M^TM=Q^T\operatorname{diag}(\lambda_1,\lambda_2)Q.$$

It follows that

$$\tilde{M} := MQ^T \operatorname{diag}(\frac{1}{\sqrt{\lambda_1}}, \frac{1}{\sqrt{\lambda_2}}),$$
$$\tilde{M_1} := M_1Q^T \operatorname{diag}(\frac{1}{\sqrt{\lambda_1}}, \frac{1}{\sqrt{\lambda_2}}),$$

satisfy

$$\tilde{M}^T\tilde{M} = I = \tilde{M_1}^T\tilde{M_1}$$

and thus $\tilde{M}, \tilde{M_1} \in SO(2)$. Here we used that $\det(M) = \det(H) > 0$. In particular,

$$\begin{aligned} M_1 &= \tilde{M_1}Q^T \operatorname{diag}(\sqrt{\lambda_1}, \sqrt{\lambda_2}), \\ M &= \tilde{M}Q^T \operatorname{diag}(\sqrt{\lambda_1}, \sqrt{\lambda_2}) \\ &= \tilde{M}\tilde{M_1}^T M_1, \end{aligned}$$

where $\tilde{M}\tilde{M_1}^T \in SO(2)$, which implies the result. □

Acknowledgements

P.C. is supported by JSPS Grant-in-Aid for Young Scientists (B) 16K21213 and partially by JSPS Innovative Area Grant 19H05131. P.C. holds an honorary appointment at La Trobe University and is a member of GNAMPA. C.Z. acknowledges a travel grant from the Simon's foundation. B.Z. would like to thank Sergio Conti for helpful discussions, and acknowledges support by the Berliner Chancengleichheitsprogramm and by the Deutsche Forschungsgemeinschaft through SFB 1060 "The Mathematics of Emergent Effects" (project 211504053).

References

[ADMD15] Virginia Agostiniani, Gianni Dal Maso, and Antonio DeSimone. Attainment results for nematic elastomers. *Proceedings of the Royal Society of Edinburgh Section A: Mathematics*, 145(4):669–701, 2015.

[Bal04] John M. Ball. Mathematical models of martensitic microstructure. *Materials Science and Engineering: A*, 378(1–2):61 – 69, 2004. European Symposium on Martensitic Transformation and Shape-Memory.

[Bha03] Kaushik Bhattacharya. *Microstructure of martensite: why it forms and how it gives rise to the shape-memory effect Oxford series on materials modeling.* Oxford University Press, 2003.

[BJ87] John M. Ball and Richard D. James. Fine phase mixtures as minimizers of energy. *Arch. Rational Mech. Anal.*, 100(1):13–52, 1987.

[BWT94] P. Bladon, M. Warner, and E.M. Terentjev. Orientational order in strained nematic networks. *Macromolecules*, 27:7067–7075, 1994.

[CD11] Pierluigi Cesana and Antonio DeSimone. Quasiconvex envelopes of energies for nematic elastomers in the small strain regime and applications. *Journal of the Mechanics and Physics of Solids*, 59(4):787–803, 2011.

[CDK07] Sergio Conti, Georg Dolzmann, and Bernd Kirchheim. Existence of lipschitz minimizers for the three-well problem in solid-solid phase transitions. *Annales de l'Institut Henri Poincaré (C) Non Linear Analysis*, 24(6):953 – 962, 2007.

[Ces10] Pierluigi Cesana. Relaxation of multiwell energies in linearized elasticity and applications to nematic elastomers. *Archive for Rational Mechanics and Analysis*, 197(3):903–923, 2010.

[CJ01] S.H. Curnoe and A.E. Jacobs. Time evolution of tetragonal-orthorhombic ferroelastics. *Physical Review B*, 64(6):064101, 2001.

[CKO+07] Y.-W. Cui, T. Koyama, I. Ohnuma, K. Oikawa, R. Kainuma, and K. Ishida. Simulation of hexagonal–orthorhombic phase transformation in polycrystals. *Acta materialia*, 55(1):233–241, 2007.

[CKZ17] S. Conti, M. Klar, and B. Zwicknagl. Piecewise affine stress-free martensitic inclusions in planar nonlinear elasticity. *Proc. R. Soc. A*, 473(2203):20170235, 2017.

[Con08] Sergio Conti. Quasiconvex functions incorporating volumetric constraints are rank-one convex. *Journal de mathématiques pures et appliquées*, 90(1):15–30, 2008.

[CPB15] Pierluigi Cesana, Paul Plucinsky, and Kaushik Bhattacharya. Effective behavior of nematic elastomer membranes. *Archive for Rational Mechanics and Analysis*, 218(2):863–905, 2015.

[CPL14] Pierluigi Cesana, Marcel Porta, and Turab Lookman. Asymptotic analysis of hierarchical martensitic microstructure. *Journal of the Mechanics and Physics of Solids*, 72:174–192, 2014.

[CT05] Sergio Conti and Florian Theil. Single-slip elastoplastic microstructures. *Archive for Rational Mechanics and Analysis*, 178(1):125–148, 2005.

[Dac07] Bernard Dacorogna. *Direct methods in the calculus of variations*, volume 78. Springer, 2007.

[DD02] Antonio DeSimone and Georg Dolzmann. Macroscopic response of nematic elastomers via relaxation of a class of SO(3)-invariant energies. *Archive for Rational Mechanics and Analysis*, 161(3):181–204, 2002.

[DM12] Bernard Dacorogna and Paolo Marcellini. *Implicit partial differential equations*, volume 37. Springer Science & Business Media, 2012.

[GR86] Vivette Girault and Pierre-Arnaud Raviart. *Finite element methods for Navier-Stokes equations. Theory and algorithms*, volume 5. Springer Series in Computational Mathematics, Springer-Verlag, Berlin, 1986.

[JCD04] Allan E. Jacobs, Stephanie H. Curnoe, and Rashmi C. Desai. Landau theory of domain patterns in ferroelastics. *Materials transactions*, 45(4):1054–1059, 2004.

[KF95] Isabel Kundler and Heino Finkelmann. Strain-induced director reorientation in nematic liquid single crystal elastomers. *Macromolecular rapid communications*, 16(9):679–686, 1995.

[Kir03] Bernd Kirchheim. Rigidity and geometry of microstructures. *MPI-MIS lecture notes*, 2003.

[KK91] Y. Kitano and K. Kifune. HREM study of disclinations in MgCd ordered alloy. *Ultramicroscopy*, 39(1-4):279–286, 1991.

[KKK88] Y. Kitano, K. Kifune, and Y. Komura. Star-lisclination in a ferro-elastic material B19 MgCd alloy. *Le Journal de Physique Colloques*, 49(C5):C5–201, 1988.

[KMŠ03] Bernd Kirchheim, Stefan Müller, and Vladimír Šverák. Studying nonlinear PDE by geometry in matrix space. In *Geometric analysis and nonlinear partial differential equations*, pages 347–395. Springer, 2003.

[MA80a] C. Manolikas and S. Amelinckx. Phase transitions in ferroelastic lead orthovanadate as observed by means of electron microscopy and electron diffraction. I. Static observations. *Physica status solidi (a)*, 60(2):607–617, 1980.

[MA80b] C. Manolikas and S. Amelinckx. Phase transitions in ferroelastic lead orthovanadate as observed by means of electron microscopy and electron diffraction. II. Dynamic Observations. *Physica status solidi (a)*, 61(1):179–188, 1980.

[MŠ98] Stefan Müller and Vladimir Šverák. Unexpected solutions of first and second order partial differential equations. In *Proceedings of the International Congress of Mathematicians*, volume 2 of *Documents, Mathematica*, pages 691–702, Berlin, 1998.

[MŠ99] Stefan Müller and Vladimír Šverák. Convex integration with constraints and applications to phase transitions and partial differential equations. *Journal of the European Mathematical Society*, 1:393–422, 1999. 10.1007/s100970050012.

[Pat14] Stuart Patching. Microstructures in the hexagonal-to-rhombic phase transformation. *OxPDE summer research project*, 2014.

[PB16] Paul Plucinsky and Kaushik Bhattacharya. Interplay of microstructure and wrinkling in nematic elastomer membranes. In *XXIV ICTAM*, 2016.

[PL13] Marcel Porta and Turab Lookman. Heterogeneity and phase transformation in materials: Energy minimization, iterative methods and geometric nonlinearity. *Acta Materialia*, 61(14):5311–5340, 2013.

[Pom10] Waldemar Pompe. Explicit construction of piecewise affine mappings with constraints. *Bulletin of the Polish Academy of Sciences. Mathematics*, 58(3):209–220, 2010.

[RTZ18] Angkana Rüland, Jamie M Taylor, and Christian Zillinger. Convex integration arising in the modelling of shape-memory alloys: some remarks on rigidity, flexibility and some numerical implementations. *Journal of Nonlinear Science*, pages 1–48, 2018.

[Rül16] Angkana Rüland. The cubic-to-orthorhombic phase transition: Rigidity and non-rigidity properties in the linear theory of elasticity. *Archive for Rational Mechanics and Analysis*, 221(1):23–106, 2016.

[RZZ18] Angkana Rüland, Christian Zillinger, and Barbara Zwicknagl. Higher Sobolev regularity of convex integration solutions in elasticity: The Dirichlet problem with affine data in int(K^{lc}). *SIAM Journal on Mathematical Analysis*, 50(4):3791–3841, 2018.

[RZZ19] Angkana Rüland, Christian Zillinger, and Barbara Zwicknagl. Higher Sobolev regularity of convex integration solutions in elasticity: The planar geometrically linearized hexagonal-to-rhombic phase transformation. *Journal of Elasticity*, pages 1–76, 2019.

[VD76] J. Vicens and P. Delavignette. A particular domain configuration observed in a new phase of the Ta-N system. *Physica status solidi (a)*, 33(2):497–509, 1976.

[WT03] Mark Warner and Eugene Michael Terentjev. *Liquid Crystal Elastomers*. International Series of Monographs on Physics. Oxford University Press, 2003.

[WWC99] Y.H. Wen, Y. Wang, and Long-Qing Chen. Effect of elastic interaction on the formation of a complex multi-domain microstructural pattern during a coherent hexagonal to orthorhombic transformation. *Acta materialia*, 47(17):4375–4386, 1999.

[ZRM09] Z. Zhang, R.D.James, and S. Müller. Energy barriers and hysteresis in martensitic phase transformations. *Acta Materialia*, 57(15):4332–4352, 2009.

Institute of Mathematics for Industry, Kyushu University, Fukuoka, Japan and Department of Mathematics and Statistics, La Trobe University, Australia
Email address: cesana@math.kyushu-u.ac.jp

Max-Planck-Institute for Mathematics in the Sciences, Inselstr. 22, 04103 Leipzig
Email address: DellaPorta@mis.mpg.de

Max-Planck-Institute for Mathematics in the Sciences, Inselstr. 22, 04103 Leipzig
Email address: rueland@mis.mpg.de

Department of Mathematics University of Southern California 3620 S. Vermont Avenue Los Angeles, CA 90089-2532
Email address: zillinge@usc.edu

Technische Universität Berlin Institut für Mathematik, Sekretariat MA 6-4, Strasse des 17. Juni 136, 10623 Berlin
Email address: zwicknagl@math.tu-berlin.de